Spring 1-1-2012

Load-Transfer Analysis of Energy Foundations

Navid Plaseied
University of Colorado at Boulder, navid.plaseied@colorado.edu

LOAD-TRANSFER ANALYSIS OF ENERGY FOUNDATIONS

by

Navid Plaseied

M.S., Amir-Kabir University of Technology, 2006

A thesis submitted to the

Faculty of the Graduate School of the

University of Colorado in partial fulfillment

of the requirement for the degree of

Master of Science

Department of Civil, Environmental and Architectural Engineering

2011

This thesis entitled:

Load-Transfer Analysis of Energy Foundations

written by Navid Plaseied

has been approved by the Department of Civil, Environmental, and Architectural Engineering

_____
Professor John S. McCartney (committee chair)

_____
Professor Dobroslav Znidarcic

_____
Professor Richard Regueiro

Date_____

The final copy of this thesis has been examined by the signatories, and we
Find that both the content and the form meet the acceptable presentation standards
Of scholarly work in the above mentioned discipline.

Plaseied, Navid (M.S. Civil Engineering, Department of Civil, Environmental, and Architectural Engineering, M.S. Rock Mechanics Engineering, Amir-Kabir University of Technology)

Load-Transfer Analysis of Energy Foundations

Thesis directed by Professor John S. McCartney

ABSTRACT

Energy foundations, or deep foundations which incorporate heat exchangers, are a novel approach to improve the energy efficiency of building heat pump systems. This study focuses on the development of a new load-transfer analysis to assess the thermo-mechanical response of energy foundations. This new analysis builds upon well-established soil-structure interaction algorithms for mechanical loading to incorporate the effects of restrained thermal expansion of the energy foundation during changes in temperature. Novel aspects include a method to evaluate the impact of increased lateral stresses on the ultimate side shear resistance due to radial expansion of the foundation, a method to track the direction of mobilized side shear stresses during thermal expansion, and a method to consider consolidation of the soil at the foundation toe during thermal expansion on the ultimate end bearing.

A parametric evaluation of the new model was performed to assess the thermo-mechanical response of different representative boundary conditions for energy foundation, including the stiffness of the soil at the toe of the foundation and the stiffness response of the overlying structure. As expected, the results indicate that the higher the temperature change, the higher the magnitudes of thermally induced axial stress and strain along the length of the foundation. The main impacts of the boundary conditions are reflected in the nonlinearity of the distribution of the thermal axial stresses and strains and the location of the maximum stress and strain (the null point). Also, it was observed that the response of energy foundation is directly related to the soil

properties, primarily the friction angle (which affects the side shear resistance) and the c/p ratio (which affects the end bearing).

Axial thermal stress distribution data from a centrifuge-scale model energy foundation were used to validate the results from the load-transfer model. In the centrifuge test, an end-bearing foundation restrained by a building load was heated in stages from 20 to 40 °C. The maximum axial thermal stress was observed in the lower half of foundation. After selecting an appropriate value for the stiffness of the loading system applying the prototype building load, the results of the load transfer analysis were found to represent the data well. The observations from the centrifuge model and the load transfer analysis were consistent with those obtained for full-scale load tests on energy foundations in the technical literature. The new load transfer analysis provides a useful design tool to evaluate stress and strain distributions in energy foundations.

ACKNOWLEDGEMENT

The author wishes to acknowledge his advisor, Professor John Scott McCartney, for his assistance, inspiration, and enthusiasm throughout my research project. Special thanks are given to Professors Dobroslav Znidarcic and Richard Regueiro for serving on my thesis committee. Deserving of additional thanks for their insight, thoughts and assistance are Ali Khosravi and Alireza Mahdian.

TABLE OF CONTENTS

1. Introduction 1

1.1 Concept of Energy Foundation 1

1.2 Problem Statement 3

1.3 Objectives and Approach 4

1.4 Scope 4

2. Literature Review 6

2.1 Thermo-Mechanical Response of Energy Foundations 6

2.2 Review of Soil-Structure Interaction Observed in Field Installations 11

2.2.1 In-situ Energy Foundation at Lambeth College (UK) 11

2.2.2 In-situ Energy Foundation at EPFL (Switzerland) 14

3. Load-Transfer Model Description 18

3.1 Mechanical Load-Transfer (T-z) Analysis 19

3.2 Thermal T-z Analysis 24

3.2.1 The Null Point Criterion 25

3.2.2 Algorithm 27

3.3 Thermo-Mechanical T-z Analysis 33

4. Definition of Thermo-Mechanical Effects on Foundation Capacity 37

4.1 Ultimate End Bearing Capacity 37

4.2 Ultimate Side Shear Resistance 40

5. Evaluation of the Load-Transfer Analysis 44

5.1 Definition of the Null point Location for Simple Cases 44

5.2 Evaluation of the Impact of Boundary Conditions on Thermal Load-Transfer 47

Analysis

5.1.1 Case 1: Semi-Floating Shaft 47

5.2.2 Floating Shaft 50

5.2.3 End-bearing Shaft 52

5.3 Impact of Temperature on the Thermo-mechanical Response of an Energy Foundation 52

5.4 Impact of Soil Friction Angle on the Thermo-Mechanical Response of an Energy Foundation 55

5.5 Impact of Head-Structure Stiffness on the Thermo-Mechanical Response of an Energy Foundation 56

6. Load-Transfer Analysis Validation 58

6.1 Model Foundation Description 58

6.2 Centrifuge Test Description 59

6.3 Soil Description 61

6.4 Centrifuge Testing Results 62

6.5 Load-Transfer Model Analysis 63

7. Conclusion 66

References 66

Appendix A 69

LIST OF TABLES

Table 5.1: Model parameters for Case 1: Semi-floating shaft 48

Table 5.2: Model parameters for Case 2: Floating shaft 49

Table 6.1: Model parameters 62

LIST OF FIGURES

Figure 1.1: Schematic representation of an energy foundation (after Laloui 2011) 2

Figure 2.1: Comparison of axial stresses induced by mechanical and thermal loading for a floating energy foundation (free at top and bottom) (after Bourne-Webb et al. 2009): (a) During heating; (b) During cooling 8

Figure 2.2: Schematic of shear resistance response for a floating energy foundation (free at top and bottom) (after Bourne-Webb et al. 2009): (a) During heating; (b) During cooling 10

Figure 2.3: Schematic mobilized side shear stress-strain paths during heating 10

Figure 2.4: Strain profiles in energy foundation at Lambeth College in London (after Bourne-Webb et al. 2009) 12

Figure 2.5: (a) Axial load and (b) Shaft resistance in energy foundation at Lambeth College in London (after Bourne-Webb et al. 2009) 13

Figure 2.6: Thermally induced displacements in the Lambeth College energy foundation 14

Figure 2.7: Measurements of strains of energy foundation (after Laloui et al. 2006): (a) During heating to 21 °C; (b) During cooling to 3 °C. 16

Figure 2.8: Axial stress distribution of energy foundation at EPFL under an axial load of 1300 kN and during heating ($\Delta T=13.4^0C$) at EPFL (after Laloui et al. 2006) 15

Figure 2.9: Thermally induced displacements in the EPFL energy foundation (after Laloui et al. 2006) 17

Figure 3.1: Discretized foundation used in the T-z Analysis 20

Figure 3.2: Typical element i along with load variables 20

Figure 3.3: Typical nonlinear spring inputs for the load transfer analysis: (a) Q-Z curve; (b) T-Z curve (Reese and O'Neill 1988) 21

Figure 3.4: Components of the mechanical load-transfer analysis 22

Figure 3.5: Typical foundation schematic of n elements highlighting the location of the null point (after Knellwolf et al. 2011) 25

Figure 3.6: Thermal load model analysis for heating 28

Figure 3.7: Thermal load model analysis for cooling 29

Figure 4.1: Load-settlement curves for three scale-model foundations in prototype scale (McCartney et al. 2010) NOTE: Test 1: Baseline loading at 15 °C; Test 2: Heating to 50 °C then loading; Test 3: Heating to 50 C°, Cooling to 20 °C then loading 38

Figure 4.2: Compression curve for Bonny silt at ambient temperature 39

Figure 4.3: The "R" envelope (i.e., $(\sigma 1-\sigma 3)f$ vs. $\sigma'3,c$) for Bonny silt, used to define the change in cu or the c/p ratio for undrained shear loading 40

Figure 4.4: Load-transfer curves: (a) Q-z curve; (b) T-z curve 42

Figure 5.1: Typical foundation schematic along with geometric and resistance load variables (for a foundation under heating) 45

Figure 5.2: Compressive stress vs. depth for a semi-floating shaft under mechanical loading (M), thermal loading (T), thermo-mechanical loading (M+T) 48

Figure 5.3: Thermo-mechanical strain vs. depth for a semi-floating shaft in Case 1 49

Figure 5.4: Compressive stress vs. depth for a floating shaft under mechanical loading (M), thermal loading (T), thermo-mechanical loading (M+T) 50

Figure 5.5: Thermo-mechanical strain vs. depth for a floating shaft 51

Figure 5.6: (a) Compressive stress (b) thermo-mechanical strain vs. depth for an end-bearing shaft 51

Figure 5.7: Change in compressive stress of a semi-floating shaft in response to different 52

temperatures

Figure 5.8: Change in axial strain of a semi- floating shaft in response to different temperatures 53

Figure 5.9: Maximum values of stress and strain in a semi-floating foundation at different temperatures 54

Figure 5.10: Impact of the soil friction angle on the mechanical behavior of a floating foundation: (a) Axial thermal stress (b) Axial thermal strain 55

Figure 5.11: Impact of the Impact of the head-structure stiffness (Kh) on the thermo-mechanical behavior of a floating foundation: (a) Axial thermal stress (b) Axial thermal strain 56

Figure 6.1: (a) Scale model foundation; (b) Schematic with instrumentation layout (Stewart and McCartney 2012) 58

Figure 6.2: Schematic of the model, container and load frame used in centrifuge testing (Stewart and McCartney 2012) 59

Figure 6.3: Section of instrumentation layout (Stewart and McCartney 2012) 60

Figure 6.4: Heat pump configuration and heat control system (Stewart and McCartney 2012) 60

Figure 6.5: Axial compressive stress profiles in different temperature changes for the centrifuge model foundation 62

Figure 6.6: The comparison between the model prediction and the experimental data at (a) $\Delta T = 5°C$; (b) $\Delta T = 10°C$; (c) $\Delta T = 15°C$; (d) $\Delta T = 19°C$ 64

CHAPTER 1: Introduction

1.1 Concept of Energy Foundations

Energy foundations include all types of foundations (deep, shallow, driven, drilled, *etc.*) which have been modified to exchange heat between a building and the subsurface using a heat pump. The heat pump is used to circulate a heat exchange fluid (i.e., typically water mixed with propylene glycol) through flexible high density polyethylene (HDPE) tubing embedded within the foundation during construction. Because the subsurface soil and rock have a relatively steady temperature approximately equal to the mean annual air temperature at a given location, the efficiency of heat exchange is higher than that obtained when using an air-source heat pump. The main advantage of energy foundations is that they provide a unique approach to reduce material and installation costs of ground-source heat exchangers, while still serving their original purpose of providing mechanical support to the building (Ooka et al. 2007). Properly designed energy foundations are expected to be a sustainable heat exchange technology, as heat extracted from the ground in the winter can be re-injected back into the ground in the summer (Brandl 2006).

Although it is possible to install heat exchangers into any foundation type, most energy foundations are cast-in-place drilled shafts. In these energy foundations, heat exchange tubing can be attached to the metallic reinforcement cage inside the concrete before it is lowered into the hole drilled in the ground. Schematic representations of different aspects of energy foundations are shown in Figure 1.1.

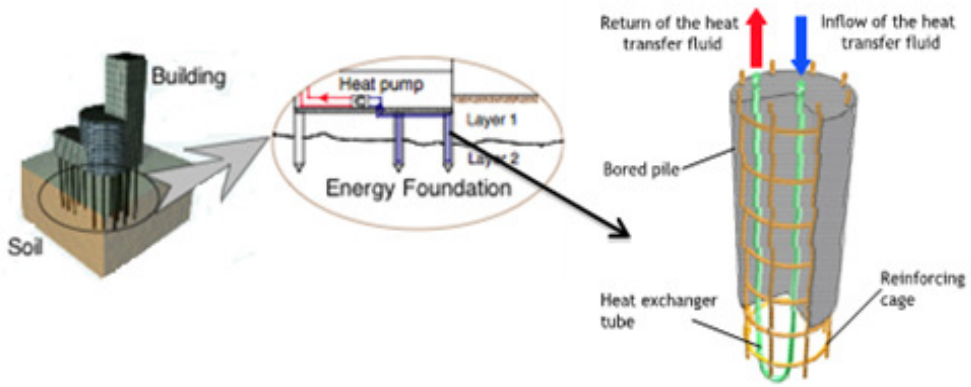

Figure 1.1: Schematic representation of an energy foundation (after Laloui 2011)

One of the first studies on the feasibility of energy foundations was by Ennigkeit and Katzenbach (2001), who summarized the heat exchange relationships required for their thermal design. Energy foundations have since been successfully implemented in buildings in Europe (Brandl 2006; Laloui et al. 2006; Adam and Markiewicz 2009), Japan (Ooka et al. 2007), and the UK (Bourne-Webb et al. 2009; Wood et al. 2009). Brandl (2006) reported that there are currently over 25,000 energy foundations in Austria since 1980, while Amis et al. (2009) reported that the installation of energy foundations has grown significantly in the UK since 2005. One of the reasons behind this rise in production is the passage of different regulations in these countries requiring the construction of zero-carbon buildings in the next 10 to 15 years. Similar targets are being set across the world implying a continued increase in production of energy foundations. In the United States there are two operational energy foundation systems to date, at the Art House in Seattle, WA, designed and constructed by Kulchin Drilling (Redmond Reporter 2010) and at the Denver Housing Authority Senior Living Facility at 1099 Osage St. in Denver, CO (Zitz and McCartney 2011).

1.2 Problem Statement

Evaluation of the long-term mechanical performance of energy foundations requires consideration of the complex interaction between temperature changes during heat exchange and induced thermo-mechanical stresses and deformations. Although no undesirable mechanical performance of energy foundations has been noted in the technical literature, their mechanical behavior and interaction with different soil profiles is not well understood. Although heating and cooling of foundations and surrounding soils are expected to lead to thermal deformations, soil-structure interaction between the soil and foundation will resist these deformations and will lead to internal stresses in the foundation. In the best-case scenario, soil-structure interaction will prevent any thermal deformations from being observed at the ground surface. However, in soil deposits like normally consolidated clays, heating may lead to elasto-plastic deformation in the surrounding soil (Abuel-Naga et al. 2009). Further, even if thermal deformations are not noted at the ground surface, the tendency for thermal deformations may lead to significant changes in the stress state in the foundation if it is constrained by a building load or mobilized side shear stresses.

Although some studies have developed preliminary soil-structure interaction analyses (Knellwolf et al. 2011) and advanced finite element models (Laloui et al. 2006), these studies have not incorporated constitutive models to consider changes in soil behavior during heating and cooling or the role of relative radial expansion of the soil and foundation. Further, the effects of radial expansion or contraction of the foundation on the ultimate side shear resistance of the foundation have not been incorporated into these

analyses. Investigation of these different issues is expected to lead to an improvement in the confidence of designers to install energy foundations in any soil profile.

1.3 Objectives and Approach

The main objective of this study is to understand the interaction between soils and energy foundations during combined mechanical and thermal loading. To reach this objective, a new load-transfer analysis is developed which can consider the different phenomena noted in the previous section. Further, this load-transfer analysis will be validated using data from a centrifuge test on a scale-model foundation heated to different temperatures.

1.4 Scope

Chapter 2 of this thesis includes a review of the current state of knowledge regarding the thermo-mechanical behavior of energy foundations. This also includes a review of hypothetical axial and mobilized side shear stress diagrams for simple boundary conditions, as well as soil-structure interaction data obtained from field installations for two case studies. Chapter 3 provides a detailed description of the algorithms for mechanical, thermal and thermo-mechanical axial load transfer (T-z) analysis. Chapter 4 involves a detailed description of the ultimate end bearing and side shear resistance values used in the T-z analysis, which provide an improvement over the T-z analysis developed by Knellwolf et al. (2011). Chapter 5 includes a parametric study to evaluate the impact of different representative boundary condition cases. This chapter includes several simple analyses to clarify the concept of the null point (the point about which the foundation expands during heating), as well as an evaluation of the impact of different boundary conditions on the stress-strain profiles in foundations with different boundary

conditions. A parametric evaluation of the impact of temperature and soil friction angle on the thermo-mechanical response of an energy foundation is also provided. Chapter 6 describes the validation of the load transfer analysis using thermal soil-structure interaction data from a small-scale centrifuge energy foundation. The complete load transfer analysis implemented in MATLAB is presented in Appendix A.

CHAPTER 2: Literature Review

2.1 Thermo-Mechanical Response of Energy Foundations

Deformations may occur in energy foundations during heating and cooling due to thermo-elastic expansion and contraction of the reinforced concrete. If the temperature changes in the foundation are uniform, both axial and radial thermo-elastic strains are expected. For afoundation which is unrestrained by the boundaries or surrounding soil, the thermo-elastic axial strain $\varepsilon_{a,T}$ is linearly proportional to changes in temperature ΔT, with a slope equal to the coefficient of linear thermal expansion α_T , as follows:

Eq. 2.1 $$\varepsilon_{a,T} = \alpha_T \Delta T$$

The coefficient of thermal expansion α_T is specific to a given material. The value of α_T for concrete can be as high as 14.5×10^{-6} m/m°C, while that of steel reinforcement members is approximately 11.9×10^{-6} m/m°C (Choi and Chen 2005). The coefficients of thermal expansion are approximately compatible, which implies that reinforced concrete will not be subject to significant differential internal stresses between the steel and concrete. The overall coefficient of thermal expansion of reinforced concrete ranges from 8.0×10^{-6} m/m°C to 10.0×10^{-6} m/m°C (Choi and Chen 2005; Bourne-Webb et al. 2009; Knellwolf et al. 2011).

Deformations are also expected in an energy foundation during initial mechanical loading associated with construction of the overlying building. The mechanical axial strain $\varepsilon_{a,M}$ in reinforced concrete is expected to be elastic under typical building loads, equal to the axial stress σ_a divided by the elastic modulus of the foundation E_f, as follow:

Eq. 2.2 $$\varepsilon_{a,M} = \sigma_a / E_f$$

The following relationship can be used to predict the overall elastic modulus of reinforced concrete in an energy foundation E_f (Laloui et al. 2006):

Eq. 2.3
$$E_f = E_{concrete}\left[1 + \varphi.\frac{E_{steel}}{E_{concrete}}\right]$$

The elastic modulus of the unreinforced concrete $E_{concrete}$ is typically obtained using laboratory compression tests. Laloui et al. (2006) measured a value of $E_{concrete}$ = 32 GPa for the concrete used in an energy foundation installed at the Ecole Polytechnique Federal de Lausanne (EPFL) in Switzerland. Laloui et al. (2006) this value and Equation (2.1) to define the elastic modulus of their energy foundation to be 29.2 GPa.

The magnitude of thermal axial expansion or contraction of an energy foundation in the ground will differ from that predicted by Eq. 2.1 because of soil-structure interaction. Specifically, because the strains at the soil-foundation interface must be compatible, the side shear resistance between the foundation and surrounding soil will restrict the thermo-elastic movement of the foundation. This interaction is complex, and depends on the soil type, the stress state in the soil, and any changes in the ultimate capacity of the foundation due to heating.

The mechanisms of thermo-mechanical soil-structure interaction for full-scale energy foundations can be investigated by evaluating data presented by Bourne-Webb et al. (2009) and Laloui and Nuth (2006). Although this data will be presented in Section 2.2, it is useful to first evaluate the theoretical stress distributions in energy foundations for simple boundary conditions. Specifically, the case of a floating foundation (i.e., where the foundation has no end bearing and soil-structure interaction is due to side shear resistance only) provides a simple situation to evaluate soil-structure interaction effects on the thermo-mechanical stress distributions in a foundation. When a mechanical load is

applied to the top (butt) of a foundation, the highest axial stress will occur at the top of the foundation, as shown in the left-hand schematics of Figure 2.1(a) and 2.1(b). The axial stress will decrease with depth due to mobilization of side shear resistance along the foundation. The axial stress will decrease to zero if the side shear resistance is sufficient to support the building load, but it may also decrease to a non-zero value if the foundation had non-zero end bearing at its tip.

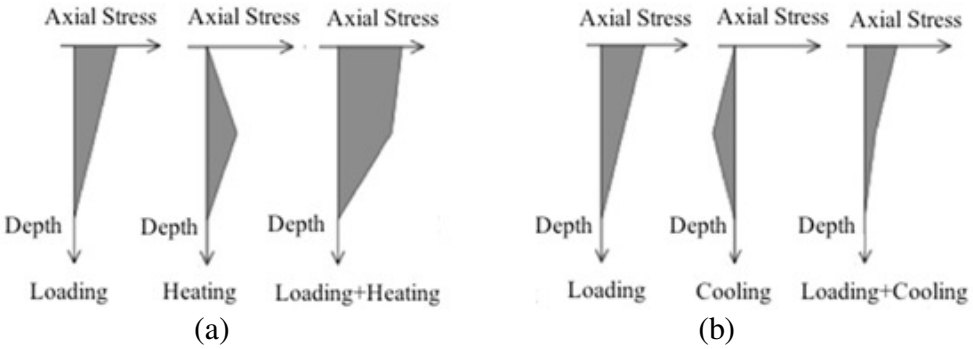

Figure 2.1: Comparison of axial stresses induced by mechanical and thermal loading for a floating energy foundation (free at top and bottom) (after Bourne-Webb *et al.* 2009): (a) During heating; (b) During cooling

During heating, a floating foundation will tend to expand about its midpoint. Because the soil side shear resistance opposes the thermal expansion of the foundation, compressive axial stresses will be generated in the foundation, as shown in the middle schematic of Figure 2.1(a). The maximum axial stress induced by heating is expected to occur in the middle of the foundation for these boundary conditions (the soil provides the most shear resistance to axial movement at this point), and will decay to zero toward the top and bottom of the foundation (Bourne-Webb et al. 2009). Further, due to the radial expansion of the foundation, the ultimate side shear which can be mobilized may increase if there is differential radial expansion between the foundation and surrounding soil leading to an increase in radial confining stress (Rosenberg 2010). When the thermally

induced stresses are superimposed atop the mechanically induced stresses, the foundation is expected to experience a net increase in compressive stress, as shown in the right-hand schematic in Figure 2.1(a).

During cooling, the opposite behavior will occur. Specifically, the foundation cooled below ambient temperatures will tend to contract about its midpoint for these boundary conditions, leading to a maximum tensile axial stress in the middle of the foundation, decaying to zero at the top and bottom of the foundation, as shown in the center schematic of Figure 2.1(b). When the thermally induced stresses are superimposed atop the mechanically induced stresses, it is possible for tensile stresses to be observed near the toe of the foundation, as shown in the right-hand schematic of Figure 2.1(b). The thermal contraction of the foundation may result in a reduction in radial confining stresses and a reduction in the ultimate side shear resistance. However, heating and cooling back to ambient conditions indicate that heating may lead to positive effects in the side-shear resistance due to consolidation of the soil surrounding the foundation (McCartney and Rosenberg 2011).

Under mechanical loading, the mobilized side shear resistance is considered to be constant along the foundation, as shown in the right hand schematics of Figures 2.2(a) and 2.2(b). During heating, upward side shear stresses will be mobilized in the lower half of the foundation while downward side shear stresses will be mobilized in the upper half of the foundation, as shown in the middle schematic of Figure 2.2(a). During cooling of the foundation, the opposite trend in mobilized side shear stresses is expected, as shown in the center schematic of Figure 2.2(b). This will lead to different side shear stress-strain paths in the upper and lower halves of the foundation.

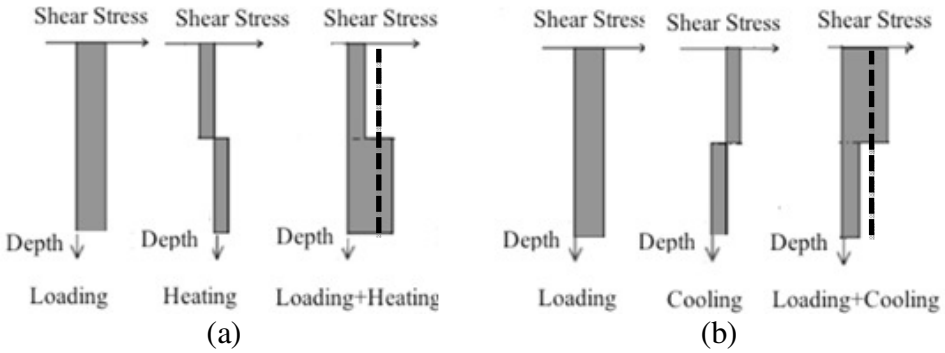

Figure 2.2: Schematic of shear resistance response for a floating energy foundation (free at top and bottom) (after Bourne-Webb et al. 2009): (a) During heating; (b) During cooling

When these mobilized side shear stresses due to thermal expansion are superimposed on the side shear stresses due to mechanical loading, the upper half of the foundation will follow an unloading path in the side shear stress-strain curve, while the lower half of the foundation will continue along the loading path in the side shear stress-strain curve. If the mobilized side shear stresses due to mechanical loading are close to the ultimate side shear resistance of the soil-foundation interface, then the lower half of the foundation may not be able to experience the full increase in mobilized side shear resistance shown in the right-hand schematic of Figure 2.2(a). This phenomenon is shown schematically in Figure 2.3.

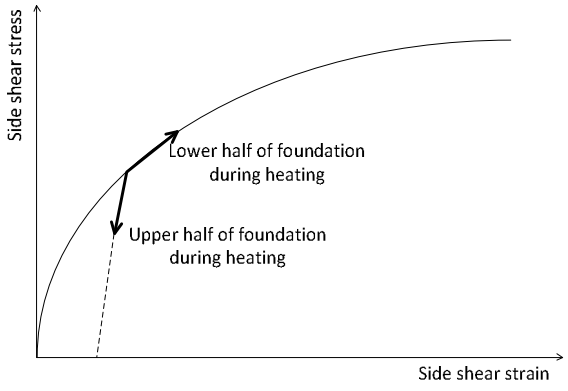

Figure 2.3: Schematic mobilized side shear stress-strain paths during heating

Bourne-Webb et al. (2009) also presented similar axial strain profiles to those shown in Figure 2.1 by considering a direct proportionality between axial stress and strain within a foundation. However, this is an issue which should be investigated further as foundations typically experience contraction due to compressive stresses induced by mechanical loading. Conversely, during thermal expansion/contraction, the compressive/tensile stresses are typically generated through foundation. The thermal expansion will result in an increase in compressive stress throughout the foundation due to the axial expansion and an increase in side shear resistance due to the radial expansion. Nonetheless, axial contraction during cooling could lead to increase in tensile stress throughout the foundation; and a decrease in ultimate side shear stress due to possible reduction in radial interface stresses.

2.2 Review of Soil-Structure Interaction Observed in Field Installations

2.2.1 In-situ Energy Foundation at Lambeth College (UK)

Bourne-Webb et al. (2009) performed a series of thermal and mechanical loading tests on a full-scale foundation in England. The foundation tested was a 0.56 m diameter drilled shaft with a depth of 22.5 meters, containing 3 polyethylene exchange loops. The lower 18.5 meters of the foundation is in London clay with the rest of the foundation in cohesionless fill material. They loaded their foundation under an initial loading stage (loading at 1200 kN), a cooling stage (with a 1200 kN mechanical load and ΔT = -19 °C from ambient) and a heating stage (maintaining the 1200 kN mechanical load, while ΔT = +10 °C from ambient).The strains were measured using vibrating-wire strain gauges (VWSGs). The strain distributions after mechanical loading and during heating and cooling are shown in Figure 2.4. The initial strain value at the bottom of the

foundation measured by Bourne-Webb et al. (2009) indicates that there was a slight mobilization of end bearing when the foundation was under loading. At the end of the cooling stage, the strain change is small in the upper 6 m of the foundation with a rapid reduction between 6 and 14 m, with tensile strains in the lower third of the foundation. At the end of the heating phase the mobilized strains are constantly larger than those prior to any temperature change (Bourne-Webb et al. 2009).

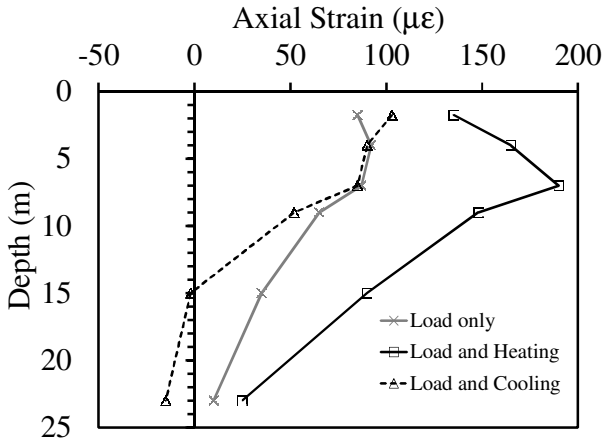

Figure 2.4: Strain profiles in energy foundation at Lambeth College in London (after Bourne-Webb et al. 2009)

During a heating cycle, axial loads/stresses in the foundation shaft are expected to be more compressive than during mechanical loading. The load and side shear resistance profiles developed from the VWSG data generally support the aforementioned mechanism as shown in Figures 2.5(a) and 2.5(b). The loading frame at the surface enables the foundation head to move freely while maintaining a constant load. The results in Figure 2.5 imply that the Lambeth College test foundation is imperfectly restrained, as the maximum apparent load is 70% higher than the load applied to the top. This contradicts the aforementioned statement that maximum thermal load is typically twice or more of the head load. There is also not much of a change in the resistance mobilized at

the foundation toe (Bourne-Webb et al. 2009).

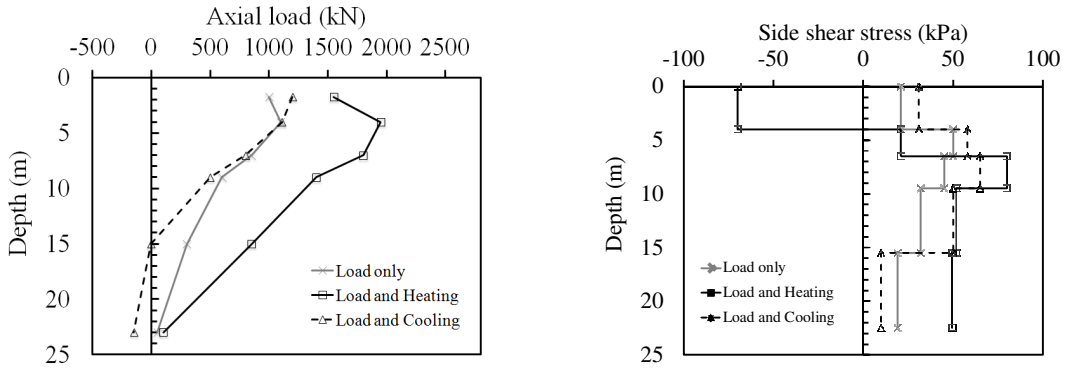

(a) (b)

Figure 2.5: (a) Axial load and (b) Shaft resistance in energy foundation at Lambeth College in London (after Bourne-Webb et al. 2009)

The discussion in the previous section also suggests that during a cooling stage applied to a foundation under mechanical loading, a reverse effect to heating should occur in which forces in the foundation generally are less compressive along with mobilizing additional side shaft resistance in the upper part of the foundation and reduced shaft resistance in the lower part of the foundation. The VWSG data support the development of these effects as shown in Figures 2.5(a) and 2.5(b), with increasing mobilized shaft resistance to about 60 kPa in the upper shaft and reducing, possibly reversing, in the lower shaft. The fluctuations in the data in the upper part of the foundation in the observed response as compared to the simplified behavior described in the previous section is perhaps due to the fact that the soil is not uniform, that is, the soil in the upper 4-5 m may be providing less resistance than the underlying clay, and may be close to its ultimate value as well. The dataset suggest that the foundation cooling led to tensile forces being developed in the lower part of the foundation, with a maximum axial tension load of 200 kN (Bourne-Webb et al. 2009).

The movement of the foundation at the ground surface for the Lambeth College test

foundation is shown in Figure 2.6. The results in this figure indicate that the foundation does move during heat exchange, but the magnitude of thermally induced movement is less than 6 mm.

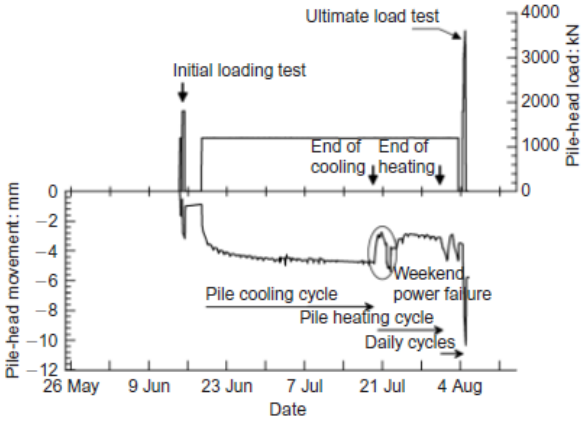

Figure 2.6: Thermally induced displacements in the Lambeth College energy foundation (Bourne-Webb et al. 2009)

2.2.2 In-situ Energy Foundation at EPFL (Switzerland)

Laloui and Nuth (2006) performed a series of thermal and mechanical loading tests on a full-scale foundation in Switzerland. The foundation tested was a 25.8 m-long drilled shaft having a diameter of 0.88 m. The upper 12 m of the foundation was in alluvial soils; where the lower part of the foundation was in glacial moraine material and the foundation was bearing on impervious Molasse material. Laloui and Nuth (2006) increased the temperature by 21 °C above the natural ground temperature, then cooled it to 3 °C above the natural ground temperature. No mechanical load was imposed at the top of the foundation, and the foundation was free to move (Test 1 as described by Laloui et al. 2006). The axial strain distributions in the foundations during heating and cooling are shown in Figure 2.7. The axial strain distribution with depth is not uniform during the heating stage and is influenced by the frictional resistance to foundation movement. The

fluctuation in axial strain measurement in the result is due to boundary condition as the foundation was installed through multiple soil layers.

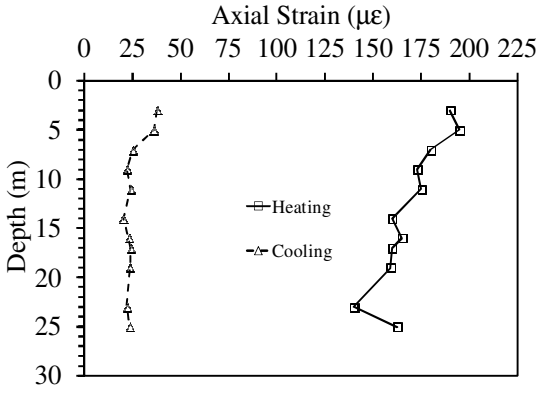

Figure 2.7: Measurements of strains of energy foundation (after Laloui et al. 2006): (a) During heating to 21 °C; (b) During cooling to 3 °C.

The axial strains during heating are more than 3 times those during cooling. Laloui and Nuth (2006) also carried out a test to examine the effects of heating and cooling on the foundation, which was confined at the top by the building (Test 7 as proposed by Laloui and et al., 2006). The observed response at the final stage of loading, with a head load of about 1300 kN, is shown in Figure 2.8 (Laloui et al. 2006). The results imply that the axial load in the foundation approximately doubled with respect to the head load during the applied thermal loading (ΔT=13.4°C). The thermal effect is more apparent at the toe of the foundation when compared to the results of Bourne-Webb et al. (2009). The overall trends in thermal axial stresses in this test are consistent with the mechanisms described in the previous section (Bourne-Webb et al. 2009).

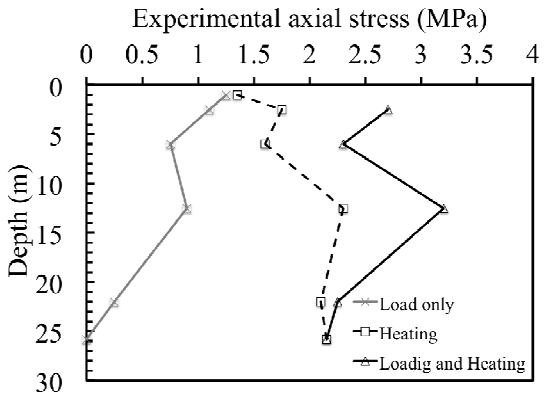

Figure 2.8: Axial stress distribution of energy foundation at EPFL under an axial load of 1300 kN and during heating (ΔT=13.4°C) at EPFL (after Laloui et al. 2006)

The most significant risk of energy foundations subject to thermo-mechanical loading is the possibility for differential movements between foundations. Asymmetric thermal expansion or contraction could lead to the generation of bending moments and differential movement (Boënnec 2009). These effects could lead to heave or settlements of the foundation butt, and could potentially create down-drag on the foundation (McCartney et al. 2010). Laloui et al. (2006) observed a butt heave of nearly 4 mm during an increase in temperature of 21 °C, as shown in Figure 2.9. The foundation did not return to its original elevation upon cooling, but maintained an upward displacement of approximately 1 mm. Laloui et al. (2006) indicated that the increase in temperature led to a plastic response in the clay. The soil was observed to partially recover deformations after cycles of heating and cooling, causing permanent measurable strains and settlements in the foundations (Laloui et al. 2006). Nonetheless, similar to the deformation results from Bourne-Webb et al. (2009) shown in Figure 2.6, the magnitude of thermal axial deformations is not significant enough to result in structural damages.

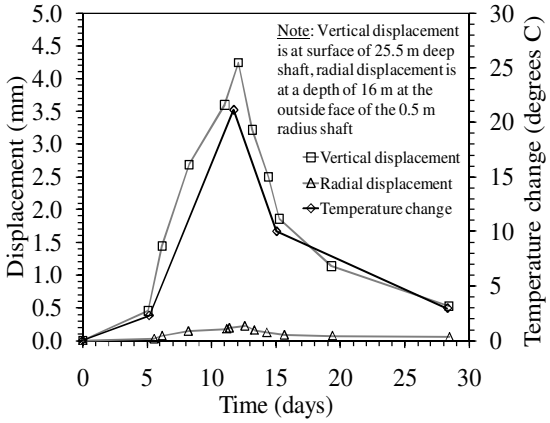

Figure 2.9: Thermally induced displacements in the EPFL energy foundation (after Laloui *et al.* 2006)

CHAPTER 3: Load Transfer Model Description

An axial load transfer (T-z) analysis is developed in this study to predict the axial deformation of an energy foundation subject to mechanical and thermal loading. Specifically, the traditional load transfer (T-z) analysis method developed by Coyle and Reese (1966), used to predict the settlement and stress distribution in deep foundations subject to mechanical loading, is extended in this study to consider thermo-elastic deformation of the foundation. The analyses are based on the following assumptions:

1. The properties of the foundation such as the Young's modulus (E) and coefficient of thermal expansion (α_T) remain constant along the foundation.
2. Downward and upward movements are taken as positive and negative respectively. Compressional stresses are also taken to be positive.
3. Foundation expands and contracts about a point referred to as the null point when it is heated or cooled (Bourne-Webb et al. 2009). The location of the null point depends on the upper and lower axial boundary conditions and side shear distribution, and will be defined later. Expansion strains are assumed to be negative.
4. Depending on the particular details of the soil profile, the ultimate side shear resistance can be assumed to be constant with depth in a soil layer (i.e., the α method) (Tomlinson 1954) or it can be assumed to increase linearly with depth in a soil profile (i.e., the β method) (Coduto 1996). Although both approaches have been implemented into the algorithm, the β method is used in the parametric study of the analysis.

   The following notations are used in the T-z analysis:

- Q is used to represent axial forces within the foundation, at the foundation base and the internal loading between the elements.
- The letter ρ stands for the relative displacement between the foundation and soil.
- K_f, K_s and K_{base} are the stiffnesses of the foundation, side shear and base spring, respectively.
- The indices "b", "t" and "s" represent the bottom, top and side of an element.
- The indices M and T stand for mechanical and thermal loading, respectively.
- The index "i" represents the element number within the foundation.
- The variable "*l*" represents the length of each element along the foundation.

3.1 Mechanical Load-Transfer (T-z) Analysis

The traditional load transfer analysis, as proposed by Coyle and Reese (1966) is used to calculate the deformation distribution within a foundation under application of a mechanical load to the foundation butt. The approach involves discretizing the foundation into a series of elements. The behavior of each foundation element can be represented by a spring with stiffness of K_i. The spring stiffness K_i is defined by the following equation:

Eq. 3.1
$$K_i = \frac{A_i E_i}{L_i}$$

where A_i is the cross section area of element i, E_i is the Young's modulus of the reinforced concrete in element i, and L_i is the length of the element. A schematic of the discretized foundation and a typical element i is shown in Figure 3.1, and the typical geometric variables are shown in Figure 3.2.

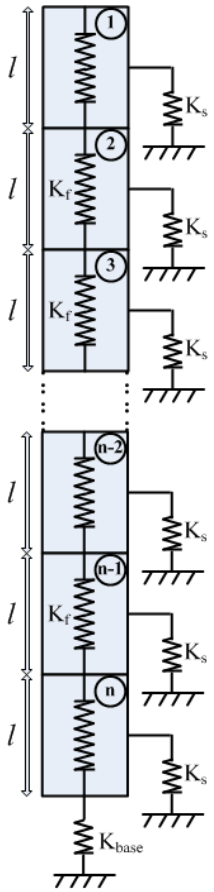

Figure 3.1: Discretized foundation used in the load transfer analysis

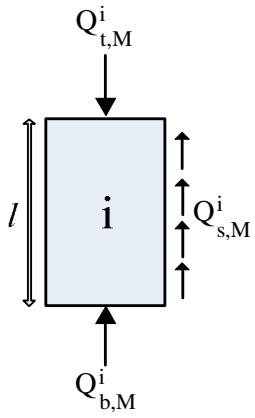

Figure 3.2: Typical element i with load variables

The displacement of the end of the foundation into the underlying soil is also represented using a nonlinear spring stiffness function referred to as a Q-z curve. Similarly, the mobilization of side shear resistance with displacement is typically

described using a nonlinear spring stiffness function referred to as a T-z curve. An example of Q-z and T-z curves for a drilled shaft foundation developed by O'Neill and Reese (1998) are shown in Figure 3.3. The ordinate of the Q-z curve is the dimensionless end bearing, which is the ratio of the actual end bearing to the ultimate end bearing, while the abscissa is the relative displacement of the foundation toe. The ordinate of the T-z curve is the dimensionless side shear, equal to the ratio of the actual shearing stress to the shearing stress at failure (ultimate side shear resistance), while the abscissa is the relative displacement between the shaft element and surrounding soil.

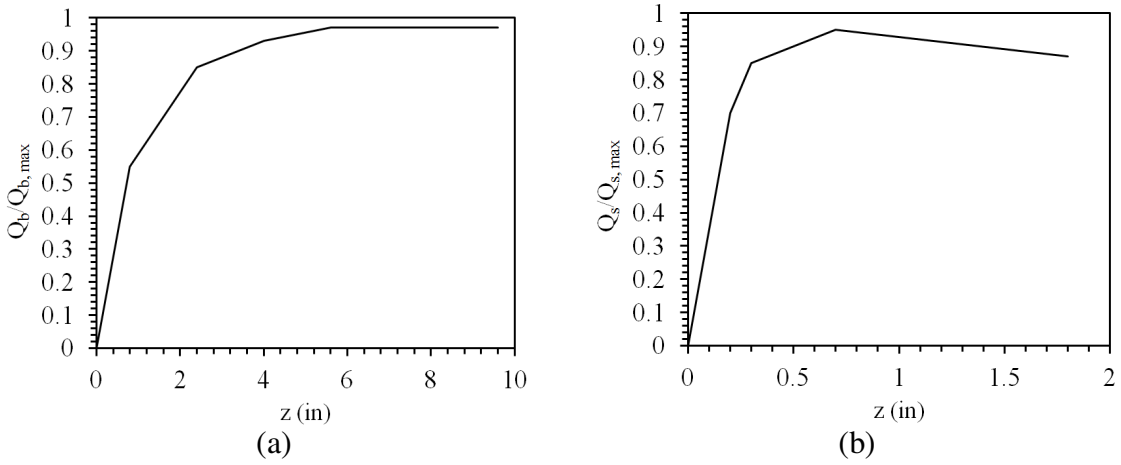

Figure 3.3: Typical nonlinear spring inputs for the load transfer analysis: (a) Q-z curve; (b) T-z curve (Reese and O'Neill 1988)

The schematics in Figure 3.4 show the discretization of the foundation for mechanical soil-structure interaction used in this study, in terms of stresses and relative displacements. The value of the displacement at the bottom of the foundation z_{base} is used to initiate the T-z analysis. The value of Q_{base} can be defined as a function of the base displacement (ρ_{base}) using the Q-z curve. Then, the axial forces acting at the top and bottom of the elements along with their displacements at the top, bottom and middle can be calculated respectively. For a foundation discretized into n elements, the axial force

acting at the bottom of element n can be defined using the Q-z curve. Specifically, the value of Q_{base} can be defined from the base displacement, which is used as an input to start the analysis. In this study, a base displacement corresponding which leads to a surface load representative of a building load was used to start the analysis.

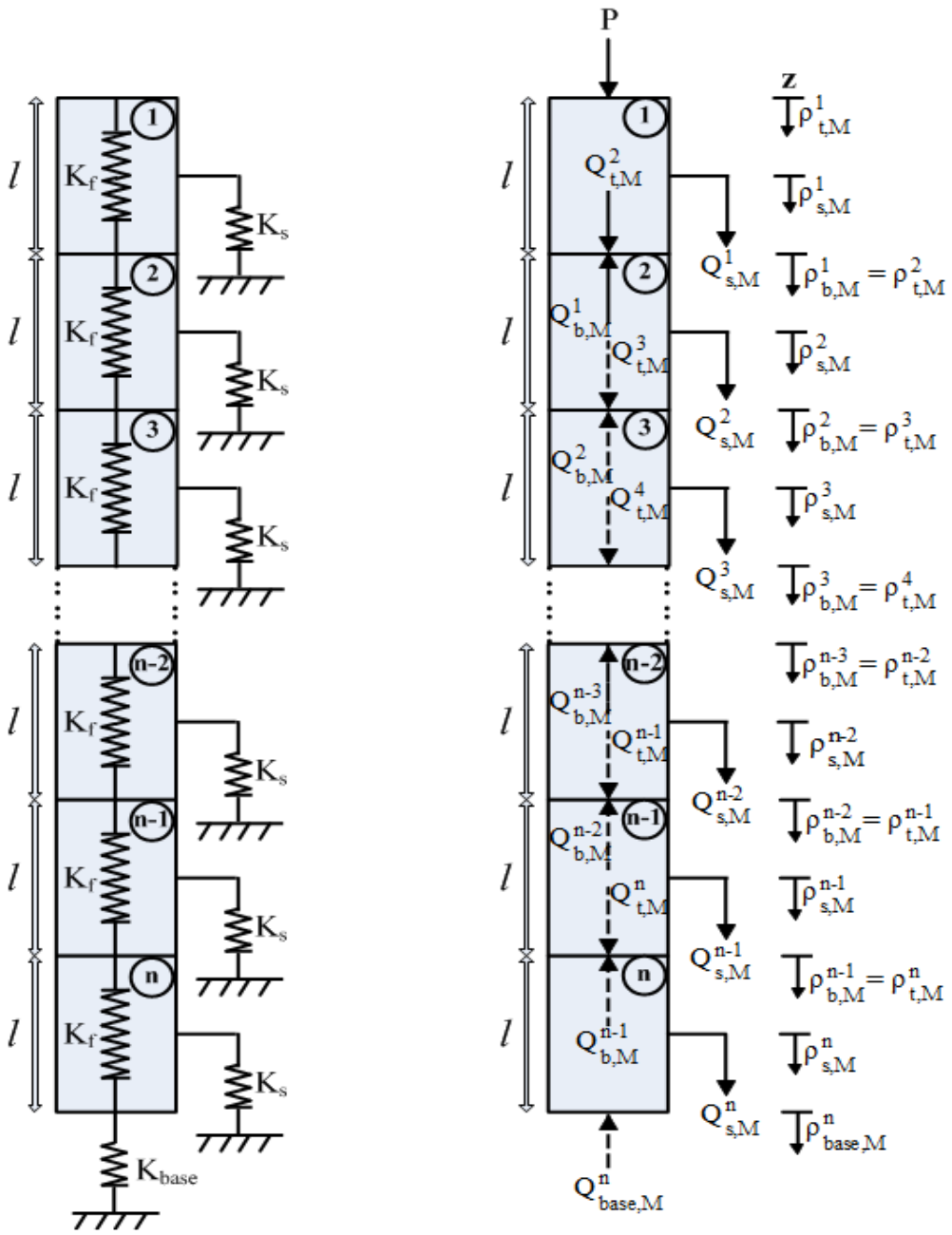

Figure 3.4: Components of the mechanical load-transfer analysis

The mechanical T-z analysis starts from element *n* (the element at the tip). Specifically, the reaction force Q_{base} can be calculated using an imposed value of ρ_{base}, as follows:

Eq. 3.2 $$Q_{base} = f(\rho_{base})$$

The average axial force in the element can be calculated by averaging the axial force at the top Q_t (initially zero) and bottom $Q_b = Q_{base}$ for element *n*. Q_{base} is the axial force acting at the bottom of element n, as follows:

Eq. 3.3 $$Q_{ave} = (\frac{Q_{b,M} + Q_{t,M}}{2})$$

Next, the elastic compression of element *n* (Δ) can be calculated by multiplying the average force Q_{ave} by the stiffness of the *K* of the element, as follows:

Eq. 3.4 $$\Delta = Q_{ave} \times K$$

Next, the displacement at the side of the element $\rho_{s,M}$ is defined by adding the settlement at the bottom of the element plus one half the elastic compression ($\frac{\Delta_M}{2}$) of the element, as follows:

Eq. 3.5 $$\rho_{s,M} = \rho_b + \frac{1}{2}\Delta_M$$

Next, the side force on the element $Q_{s,M}$ is then defined using the T-z curve and the displacement at the side $\rho_{s,M.}$ calculated using Eq. 3.5, as follows:

Eq. 3.6 $$Q_{s,M} = f(\rho_{s,M})$$

Finally, a new force at the top of the element $Q_{t,M,new}$ is defined by adding the force at the base of the element and the force on the side of the element to establish equilibrium, as follows:

Eq.3.7 $$Q_{t,M,new} = Q_{b,M} + Q_{s,M}$$

If the difference between the new and old forces on the top of the element is not less than a user-defined tolerance (a value of $10^{-6}$was used in this study) then the new axial at the top of the foundation is used to calculate a new average axial stress (Equation 3.3) and the process is repeated iteratively until convergence. The starting force for the top of the element for the each successive iteration is set equal to that of the previous iteration. If the difference is less than 10^{-6} then the processes is repeated for the next element until the top of the foundation is reached.

The force on the bottom of a subsequent element $Q_{b,M}^{i-1}$ is equal to the new force on the top of the next element $Q_{t,M}^{i}$ and the settlement on the bottom of subsequent element $\rho_{b,M}^{i-1}$ is equal to the settlement of the next element $\rho_{b,M}^{i}$ plus the elastic compression of the foundation element ($\Delta_{\mathrm{M}}^{\mathrm{i}}$), as follows:

Eq. 3.8 $$Q_{b,M}^{i-1} = Q_{t,M}^{i}$$

Eq. 3.9 $$\rho_{b,M}^{i-1} = \rho_{b,M}^{i} + \Delta_{\mathrm{M}}^{\mathrm{i}}$$

Where the value of $\rho_{b,M}$ is equal to the value of $\rho_{t,M}$ defined for the lower element. The final load on the top of the foundation $Q_{t,M}$ will cause the corresponding displacement at the top of the foundation $\rho_{t,M}$.

3.2 Thermal T-z Analysis

The load transfer (T-z) analysis method can also be used to predict the settlement and stress distribution in energy foundations subject to thermal loading (i.e., without mechanical loading). In this regard, a spring should be added to the top of the foundation,

which represents the foundation head-structure stiffness (Knellwolf et al. 2011). The "null point" location is an important variable to define in this process needed to define the thermal response of the energy foundation during heating/cooling.

3.2.1 The Null Point Criterion

Once a foundation is heated or cooled, it begins to expand or contract about its null point (Bourne-Webb et al. 2009). The null point is the location in the foundation where there is no thermal expansion or contraction, assuming that the temperature change occurs uniformly throughout the foundation. A schematic of a typical foundation divided into n equal elements, along with the location of the null point, is shown in Figure 3.5.

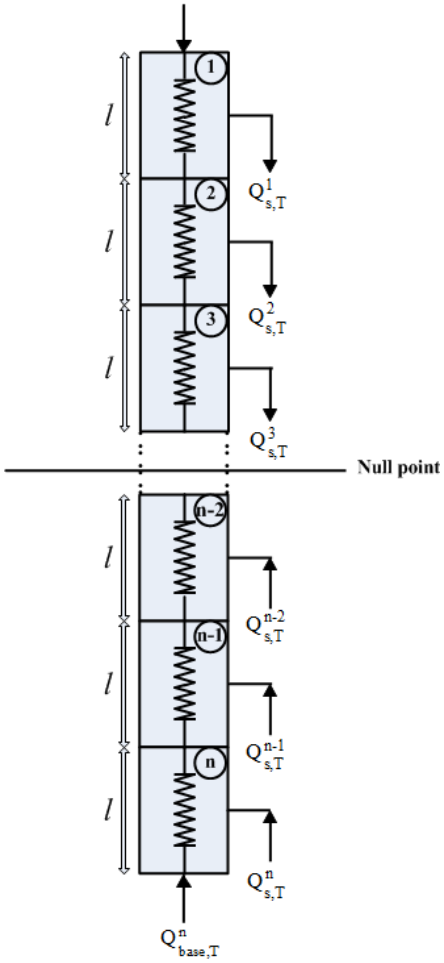

Figure 3.5: Typical foundation schematic of n elements highlighting the location of the null point (after Knellwolf et al. 2011)

In order for the displacement at the null point (denoted as NP) to be zero, the sum of the mobilized shear resistance and the structure reaction for the upper section of the null point should be equal to the sum of the mobilized shear resistance and the base reaction in the lower one (Knellwolf et al. 2011). Eq. 3.10 through Eq. 3.13 can be used to define the null point location along the foundation.

Eq. 3.10 $$\sum_{i=1}^{NP} Q_{s,T}^{i} + Q_{h,T} = \sum_{i=NP+1}^{n} Q_{s,T}^{i} + Q_{base,T}$$

Eq. 3.11 $$Q_{h,T} = f(\rho_h, K_h)$$

Eq. 3.12 $$Q_{base,T} = f(\rho_{base}, K_{base})$$

Eq. 3.13 $$Q_{s,T}^{i} = f(\rho_s^i, K_s)$$

In these equations, $Q_{base,T}$ represents the base response to the thermal expansion and contraction is defined using Q-z curve. $Q_{h,T}$ signifies the structure response is linearly proportional to the relative displacement of the head (butt) of the foundation. $Q_{s,T}^{i}$ is the shear resistance of the foundation and can be determined according to the T-z curve. K_s is the stiffness of the material surrounded energy foundation that can be constant for a single soil layer or varied in multiple soil layers. K_h represents the foundation head-structure stiffness, which depends on several factors including the rigidity of the supported structure, the type of contact between the foundation and the mat or raft, and the position and the number of energy foundations (Knellwolf et al. 2011). K_{base} is the base material stiffness and depends on the initial slope of the Q-z curve. For the case of linear elastic material at the base of foundation, K_{base} is constant. The values of ρ_h and

ρ_{base} represent the relative displacements at the head and the base of the foundation. ρ_s^i is the relative displacement at the side of the element i. The null point location for hypothetical foundations with different boundary conditions will be discussed in Sections 5.1 and 5.2.

3.2.2 Algorithm

During heating or cooling, the foundation will expand or contract about the null point. The compressional/tensile forces acting on each element restrict the movements. These induced forces initiate from the base reaction, the structure reaction and the mobilized friction forces of the adjacent elements in the foundation. The relevant variables in the thermal load transfer analysis are defined in Figures 3.6 and 3.7 for heating and cooling, respectively.

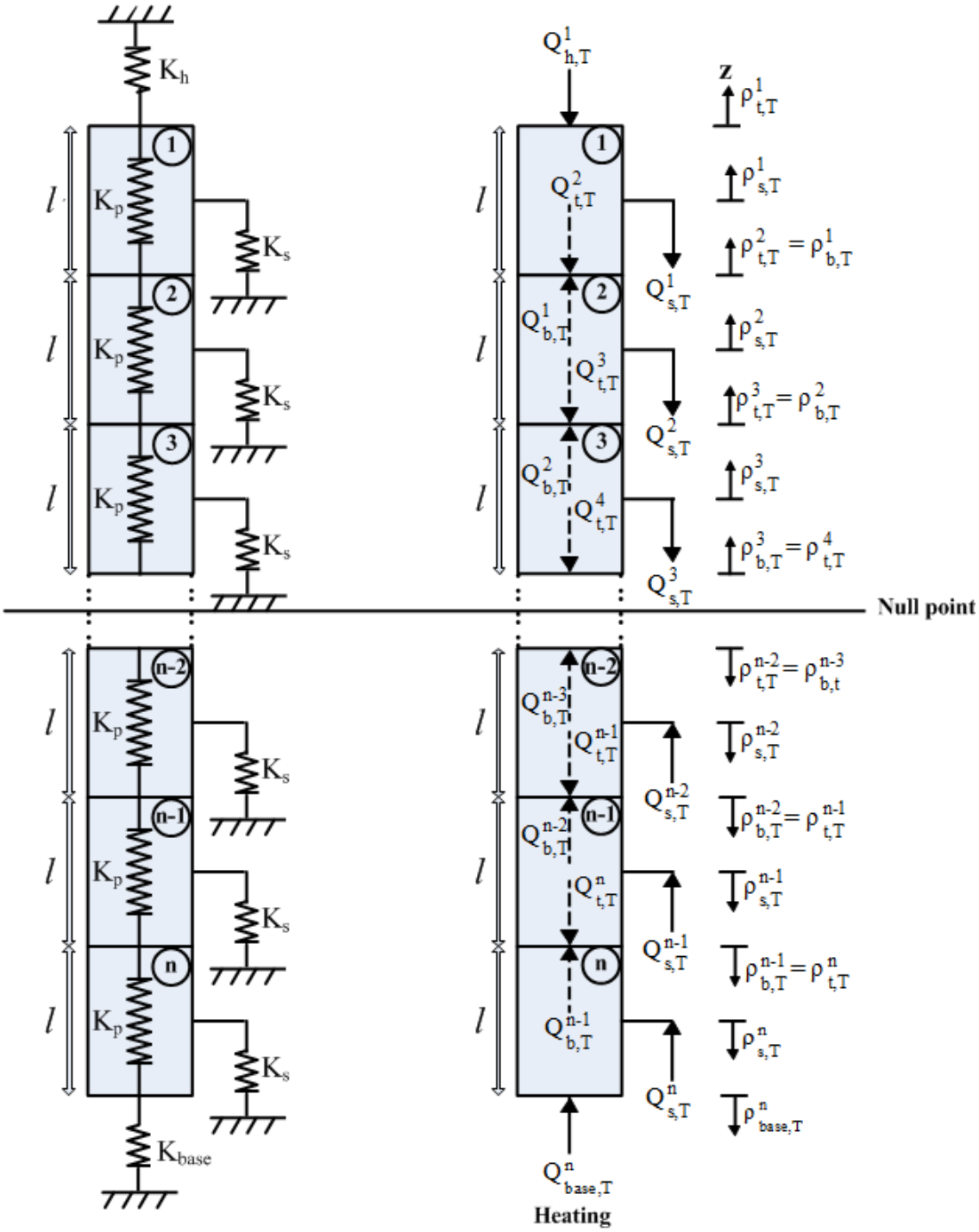

Figure 3.6: Thermal load model analysis for heating

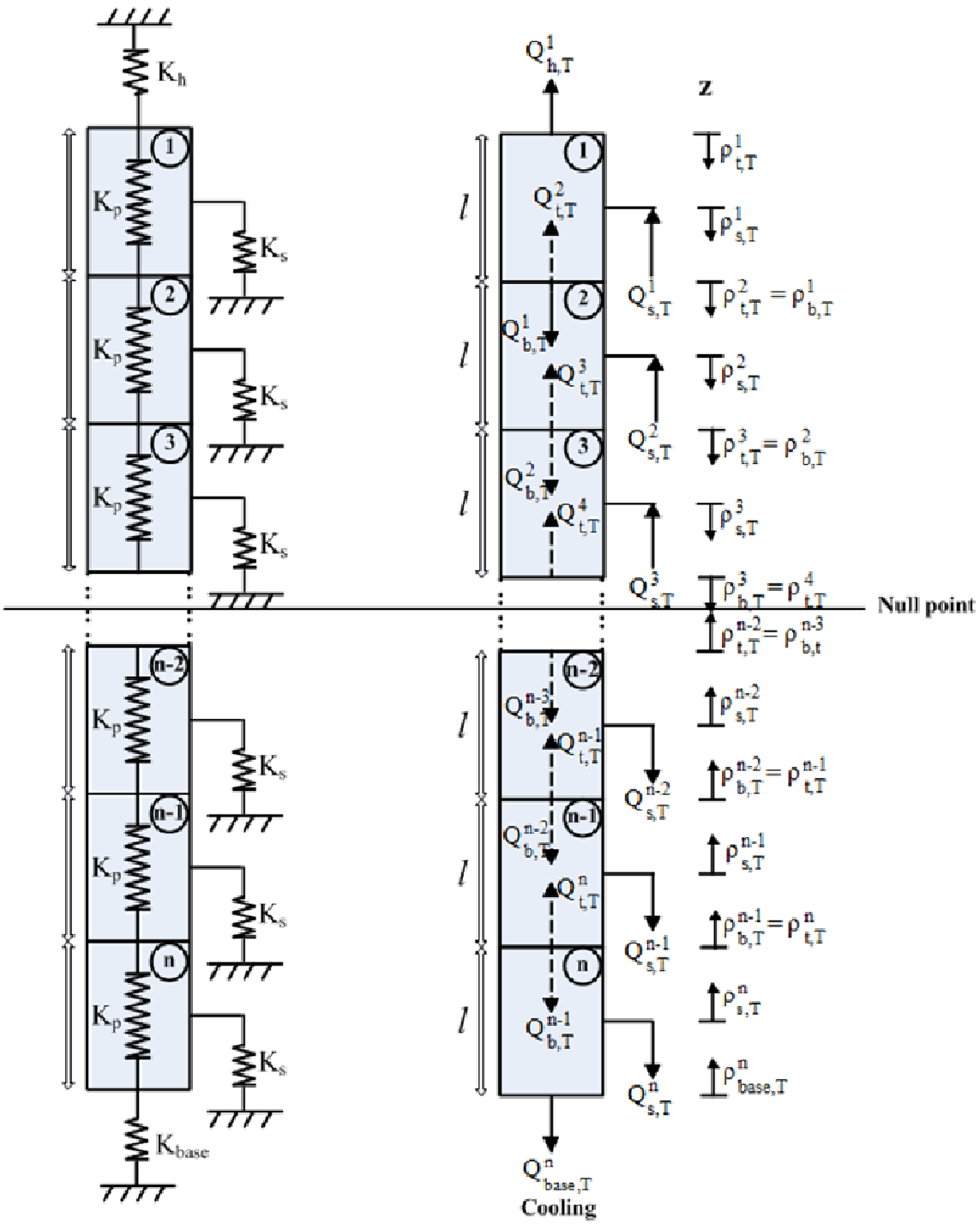

Figure 3.7: Thermal load model analysis for cooling

To compute the first set of mobilized shear resistance and the base reaction, the foundation is assumed to be totally free to move (Knellwolf et al. 2011). Therefore the

first set of displacements can be derived using following expression which l is the length of the element and i represents the element number along the foundation (i = 1 to n).

Eq. 3.14 $$\Delta_T^i = l\alpha\Delta T$$

These displacements are restricted by the surrounding soil which applies additional forces tending to compress/expand the element during heating/cooling process. The null point can be located in any element along the foundation where the null point criterion is satisfied. The first element below the null point (noted as NP+1) has no displacement at its top and it expands/contracts from the bottom during heating/cooling.

Eq. 3.15 $$\rho_{t,T}^{NP+1} = 0$$

The thermal settlement at the side and the bottom of this element can be defined using the following two equations.

Eq. 3.16 $$\rho_{s,T}^{NP+1} = \pm\frac{\Delta_T^{NP+1}}{2}$$

Eq. 3.17 $$\rho_{b,T}^{NP+1} = \pm\Delta_T^{NP+1}$$

In Eq. 3.16 and 3.17, the upper sign is used when a foundation is heated, and the lower sign is used when a foundation is cooled. The relative displacements for the rest of the elements below the null point (i = NP+2 to n) following equation can be calculated using the following equations:

Eq. 3.18 $$\rho_{t,T}^{i} = \rho_{b,T}^{i-1}$$

Eq. 3.19 $$\rho_{s,T}^{i} = \rho_{t,T}^{i} \pm \frac{\Delta_T^i}{2}$$

Eq. 3.20 $$\rho_{b,T}^{i} = \rho_{t,T}^{i} \pm \Delta_T^i$$

When the base of the foundation is reached, the first set of base reaction force along with the compressional/tensile stress acting on each element during heating/cooling can be calculated using the Eq. 3.21 through Eq. 3.24 (i = NP+1 to n):

Eq. 3.21 $$Q_{base,T} = f(\rho_{b,T,n})$$

Eq. 3.22 $$Q_{t,T}^{i} = Q_{base,T} + \sum_{j=n}^{i} Q_{s,T}^{j}$$

Eq. 3.23 $$Q_{b,T}^{i} = Q_{t,T}^{i+1}$$

Eq. 3.24 $$\sigma_i = \frac{Q_{ave}}{A} = \frac{(Q_{t,T}^{i} + Q_{b,T}^{i})}{2A}$$

After the forces acting on each element are defined, the next step is to define the actual displacement of each element using the following equation:

Eq. 3.25 $$\Delta_{Tactual}^{i} = \Delta_{T}^{i} - \frac{\sigma_i . l}{E}$$

The actual displacement in each element will be lower than that present when the foundation is free to move from the bottom. This actual displacement should be replaced with the initial displacements (free boundary) in the Eq. 3.16 through Eq. 3.20 in order to get a new actual displacement from Eq. 3.25 and this process should be repeated until the values of actual displacements reasonably converge (the difference between the new and old actual displacement is less than 10^{-6}).

For the elements above the null point (noted as NP-1, NP-2, etc.), Eqs. 3.26 through3.36 are used in the analysis. To compute the first set of mobilized friction and the structure reaction, the foundation is assumed to be totally free to move and therefore the first set of displacements can be derived using Eq. 3.26:

Eq. 3.26 $$\Delta_T^i = l\alpha\Delta T$$

The first element above the null point has no displacement at the bottom and it expands/contracts from the top during heating/cooling (Eq. 3.27).

Eq. 3.27 $$\rho_{b,T}^{NP-1} = 0$$

The thermal settlement at the side and the bottom of this element can be defined using Eq. 3.28 and Eq. 3.29 respectively.

Eq. 3.28 $$\rho_{s,T}^{NP-1} = \pm\frac{\Delta_T^{NP-1}}{2}$$

Eq. 3.29 $$\rho_{b,T}^{NP-1} = \pm\Delta_T^{NP-1}$$

Relative displacement for the rest of elements above the null point (i = NP-2 to 1) can be defined using Eq. 3.30 through Eq. 3.32.

Eq. 3.30 $$\rho_{b,T}^{i} = \rho_{t,T}^{i+1}$$

Eq. 3.31 $$\rho_{s,T}^{i} = \rho_{b,T}^{i} \pm \frac{\Delta_T^i}{2}$$

Eq. 3.32 $$\rho_{t,T}^{i} = \rho_{b,T}^{i} \pm \Delta_T^i$$

While the top of the foundation is reached, the first set of structure reaction force and also the compressional/tensile stress acting on each element above the null point (i=NP-1 to 1) during heating/cooling can be calculated using the Eq. 3.33 through Eq. 3.36:

Eq. 3.33 $$Q_{structure,T} = f(\rho_{t,T,1})$$

Eq. 3.34 $$Q_{b,T}^{i} = Q_{h,T} + \sum_{j=1}^{i} Q_{s,T}^{j}$$

Eq. 3.35 $$Q_{t,T}^{i} = Q_{b,T}^{i-1}$$

Eq. 3.36
$$\sigma_i = \frac{Q_{ave}}{A} = \frac{(Q^i_{t,T} + Q^i_{b,T})}{2A}$$

After the stress acting on each element is defined, the next step is to define the actual displacement of each element using Eq. 3.37.

Eq. 3.37
$$\Delta^i_{Tactual} = \Delta^i_T - \frac{\sigma_i . l}{E}$$

Again, these actual displacements for the top section should be replaced with the initial displacements (free boundary) in the equations Eq. 3.28 through Eq. 3.32 and the whole process should be repeated until the values of actual displacements reasonably converge (the difference between the new and old actual displacement is less than 10-6).

3.3 Thermo-Mechanical T-z Analysis

The most accurate representation of energy foundations can be obtained using a thermo-mechanical analysis, in which the thermal loading is applied to a foundation under an initial mechanical load. To calculate the thermo-mechanical response of the energy foundation, the first step is to calculate the distribution in axial and interface displacements and forces along the foundation for a given initial mechanical loading. Then the foundation response due to thermal loading (heating/cooling) will be applied subsequently to define the overall response of a foundation subject to thermo-mechanical loading. The thermo-mechanical process should be started from the "null point". Opposite to the thermal algorithm, this algorithm starts from non-zero relative displacement about the null point. Similar to thermal algorithm, the initial displacements are considered to be the same as free boundary condition ($\Delta^i_T = l\alpha\Delta T$). Eqs. 3.38 through 3.40 are used for the first element below the null point (the upper and the lower sign in following equations is used for a foundation which is heated or cooled respectively):

Eq. 3.38 $$\rho_{t,M,T}^{NP+1} = \rho_{t,M}^{NP+1}$$

Eq. 3.39 $$\rho_{s,M,T}^{NP+1} = \rho_{s,M}^{NP+1} \pm \frac{\Delta_T^{NP+1}}{2}$$

Eq. 3.40 $$\rho_{b,M,T}^{NP+1} = \rho_{b,M}^{NP+1} \pm \frac{\Delta_T^{NP+1}}{2}$$

The relative displacements for the rest of elements below the null point (i=NP+2 to n), can be defined using Eqs. 3.41 through3.43.

Eq. 3.41 $$\rho_{t,M,T}^{i} = \rho_{b,M,T,i-1}$$

Eq. 3.42 $$\rho_{s,M,T}^{i} = \rho_{t,M,T}^{i} \pm \frac{\Delta_T^{i}}{2}$$

Eq. 3.43 $$\rho_{b,M,T}^{i} = \rho_{t,M,T}^{i} \pm \Delta_T^{i}$$

While the base of the foundation is reached, the first set of base reaction force and also the compressive/tensile forces acting on each element during heating/cooling can be calculated. Before calculating these stresses the process should continue to define the relative displacements for the elements above the null points by using following equations. Specifically, Eqs. 3.44 through 3.46 are used for the first element above the null point (the top/bottom sign in following equations is used for a foundation which is heated/cooled, respectively):

Eq. 3.44 $$\rho_{b,M,T}^{NP-1} = \rho_{b,M}^{NP-1}$$

Eq. 3.45 $$\rho_{s,M,T}^{NP-1} = \rho_{b,M,T}^{NP-1} \mp \frac{\Delta_T^{NP+1}}{2}$$

Eq. 3.46 $$\rho_{t,M,T}^{NP-1} = \rho_{b,M,T}^{NP-1} \mp \Delta_T^{NP+1}$$

For the rest of elements above the null point (i = NP-2 to 1), Eq. 3.47 through 3.49 can be used:

Eq. 3.47 $$\rho_{b,M,T}^{i} = \rho_{t,M,T}^{i+1}$$

Eq. 3.48 $$\rho_{s,M,T}^{i} = \rho_{b,M,T}^{i} \mp \frac{\Delta_{T,i}}{2}$$

Eq. 3.49 $$\rho_{t,M,T}^{i} = \rho_{b,M,T}^{i} \mp \Delta_{T,i}$$

To calculate the actual displacement of each element, the compressive/tensile forces acting on each element can be defined using Eqs. 3.50 through 3.54.

Eq. 3.50 $$Q_{base,M,T} = f(\rho_{b,T,n})$$

Eq. 3.51 $$Q_{t.M,T}^{i} = Q_{base,T} + \sum_{j=n}^{i} Q_{s.M,T}^{j}$$

Eq. 3.52 $$Q_{b.M,T}^{i} = Q_{t.M,T}^{i+1}$$

Eq. 3.53 $$\sigma_i = \frac{Q_{ave}}{A} = \frac{(Q_{t.M,T}^{i+1} + Q_{b.M,T}^{i})}{2A}$$

Eq. 3.54 $$\Delta_{M,Tactual} = \Delta_{T,i} - \frac{\sigma_i . l}{E}$$

The axial force calculations should start from the base, up to the element of interest (j= n to i, where i is the element number). The mobilized side shear forces due to thermal expansion ($Q_{s.M,T}^{j}$) for the elements above the null point of the foundation will follow an unloading path in the T-z curve, while that for the elements below the null point will continue along the loading path. To determine for the elements above the null point the unloading path of the T-z curve should be used. The value of $Q_{s.M,T}^{j}$ for the elements below the null point can be defined using the loading path of the T-z curve. The actual

displacement calculated using Eq. 3.54 should be replaced with the initial displacements (free boundary) in Eqs. 3.39 through 3.49 in order to get a new actual displacement and this process should be repeated until the values of actual displacements reasonably converge (the difference between the new and old actual displacement is less than 10^{-6}). The MATLAB code in Appendix A has been thoroughly annotated to provide further information on the aspects of the different load transfer analyses.

CHAPTER 4: Definition of Thermo-Mechanical Effects on Foundation Capacity

4.1 Ultimate End Bearing Capacity

When a foundation is heated under a mechanical load (e.g., a building load), it is able to react against the building load causing the soil at the toe to consolidate. This leads to a higher end bearing capacity than a foundation which is heated to a similar temperature without a building load (Coccia et al. 2011). This idea should be incorporated in the thermo-mechanical analysis of a foundation after the first cycle of heating and cooling. In such cases, the soil at the toe of the foundation will consolidate, leading to a higher undrained shear strength (c_u) of the soil beneath the toe, which will result in a higher end bearing capacity of the foundation.

The ultimate end bearing $Q_{b,max}$ for the foundation can be defined as follows:

Eq. 4.1 $$Q_{b,max} = N_c c_u A_b$$

where N_c is the untrained bearing capacity factor for deep foundations (i.e., equal to 9 for a foundation with a circular or square cross-section and a tip depth greater than 2 foundation diameters), c_u is the undrained shear strength of the soil at the foundation tip, and A_b is the cross sectional area of the shaft toe.

The main input of the mechanical T-z analysis is the settlement of the toe of the foundation. Although the Q-z curve indicates that the mobilized end bearing will increase during mechanical loading, it is expected that the foundation will be maintained at this displacement. Although the ultimate end bearing in Eq. 4.1 represents the case of undrained loading, it is assumed that the soil at the toe of the foundation will eventually drain and undergo compression leading to a corresponding increase in undrained shear strength and ultimate end bearing capacity. Further, if the foundation is heated, one of the

outputs of the thermo-mechanical T-z analysis is the additional settlement of the toe of the foundation. An example of this phenomenon is shown in the data from McCartney et al. (2010) in Figure 4.1. For Test 2, it is clear that the foundation experienced thermo-mechanical settlement under application of an axial load of 800 kN, which contributed to the increase in foundation capacity when it was loaded to failure after heating. For Test 3, which was heated then cooled, the compression of the soil at the toe during mechanical loading and heating led to a higher foundation capacity even though it had been cooled back to the same temperature as Test 1.

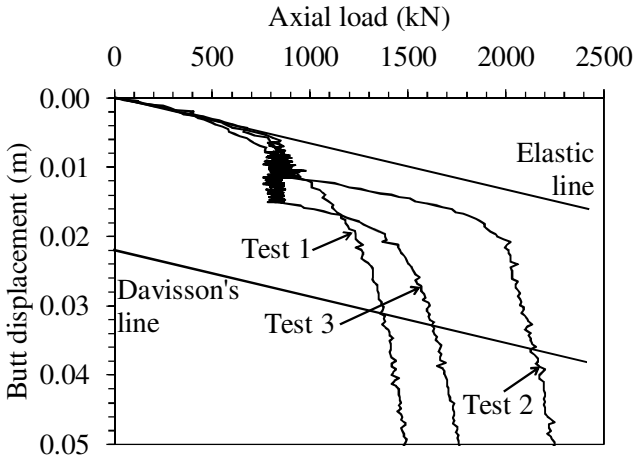

Figure 4.1: Load-settlement curves for three scale-model foundations in prototype scale (McCartney et al. 2010) NOTE: Test 1: Baseline loading at 15 °C; Test 2: Heating to 50 °C then loading; Test 3: Heating to 50 C°, Cooling to 20 °C then loading

The settlement of the foundation after the first thermo-mechanical loading calculated with the load transfer analysis can be used to estimate the change in void ratio of the soil under the toe of the foundation, as follows:

Eq. 4.2
$$\Delta e = \frac{S(1+e_0)}{H_0}$$

where H_0 is the thickness of the soil layer beneath the foundation in which there is a change in stress during heating (1 to 2 foundation diameters), e_0 is the initial void ratio, S

is the settlement of the toe of the foundation, and Δe is the change in void ratio.

The data from Bonny silt can be used as an example of how the change in void ratio can be used to estimate the increase in end bearing of the foundation. The compression curve (i.e., the relationship between e and log $\sigma'_{3,c}$) can be used to estimate the corresponding change in effective consolidation stress $\sigma'_{3,c}$. The e - log $\sigma'_{3,c}$ curve shown in Figure 4.2 was obtained from an oedometer test on Bonny silt.

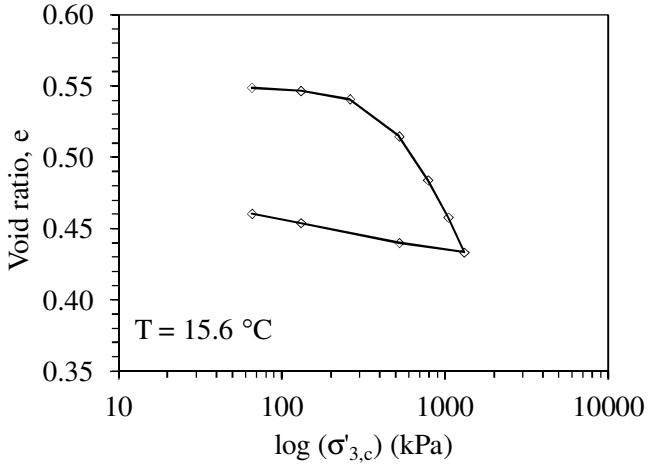

Figure 4.2: Compression curve for Bonny silt at ambient temperature

The change in effective consolidation stress can be used to estimate the change in the undrained strength of the soil using data from a consolidated undrained test. Specifically, the R-envelope, or a plot of the principal stress difference at failure $(\sigma_1-\sigma_3)_f$ vs. the effective consolidation stress $(\sigma'_{3,c})$ can be used to estimate the change in undrained shear strength of the soil. The R-envelope from a CU triaxial test on Bonny silt is shown in Figure 4.3. The change in $(\sigma_1-\sigma_3)_f$ can be predicted from the change in effective consolidation stress $(\Delta\sigma'_{3,c})$ defined from Figure 4.2 for the given change in void ratio calculated using Eq. 4.2.

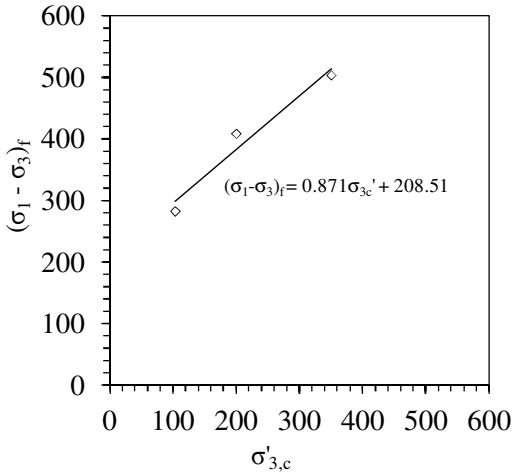

Figure 4.3: The "R" envelope (i.e., $(\sigma_1-\sigma_3)_f$ vs. $\sigma'_{3,c}$) for Bonny silt, used to define the change in c_u or the c/p ratio for undrained shear loading

The value of $\Delta(\sigma_1-\sigma_3)_f$ defined from Figure 4.2 corresponds to the change in undrained shear strength of the soil (Δc_u) as follows:

Eq. 4.3
$$\Delta c_u = \frac{\Delta(\sigma_1 - \sigma_3)_f}{2}$$

The change in undrained shear strength of the soil can then be used to calculate the increase in ultimate end bearing resistance of the foundation. This feature of the model can be used to estimate the

4.2 Ultimate Side Shear Resistance

The ultimate side shear resistance at ambient temperature conditions at a given depth can be calculated using the following equation:

Eq. 4.4
$$Q_{s,max} = \sum_{i=1}^{j} \beta A_s \sigma_v'(z(j)) K_0 tan\phi'$$

where j represents the element of interest within the foundation, β is an empirical reduction factor representing soil-interface behavior, A_s is the surface area of the

foundation sides, $\sigma_v'(z)$ is the effective overburden pressure at a given depth z, K_o is the coefficient of lateral earth pressure at rest and can be defined using following equation:

Eq. 4.5 $$K_0 = 1 - sin\emptyset'$$

where ϕ' is the drained friction angle. This empirical approach to define the ultimate side shear resistance of the foundation is referred to as the β method (Coduto 1996), and the value of β must be defined using proof tests. Rosenberg (2011) found that a value of β = 0.55 was suitable to represent the behavior of a scale-model drilled shaft in a soil having ϕ = 32°. The β method was selected for this analysis because it is an effective stress-based approach to define the side shear resistance, and heating is assumed to occur slowly leading to drained conditions in the soil. Specifically, as the foundation expands into the soil during heating, the soil will consolidate and lead to an increase in ultimate side shear resistance of the foundation. The impact of temperature on $Q_{s,max}$ due to the thermally induced radial expansion of the foundation can be determined as follows (McCartney and Rosenberg 2011):

Eq. 4.6 $$Q_{s,max} = \sum_{i=1}^{j} \beta A_s \sigma_v'(z(j)) \left[K_0 + \left(K_p - K_0\right) K_T\right] tan\phi'$$

where K_p is the coefficient of passive earth pressure and can be defined as follows:

Eq. 4.7 $$K_p = \frac{1 + sin\emptyset'}{1 - sin\emptyset'}$$

K_T is a reduction factor representing the mobilization of passive earth pressure with thermal-induced strain, equal to:

Eq. 4.8 $$K_T = \kappa \alpha_T \Delta T \left(\frac{D/2}{0.02L}\right)$$

where κ is an empirical coefficient representing the soil resistance to expansion of the foundation and maybe a stress-dependent variables, but it was assumed to be constant and equal to 65 for this parametric analysis. α_T is the coefficient of thermal expansion of reinforced concrete (9.7×10^{-6} m/m °C). The geometric normalizing factor [(D/2)/0.02L] was proposed by Reese et al. (2006).

The Q-z and T-z curves used in this study are shown in Figure 4.4(a) and 4.4(b), respectively. Although the shear strength data of Uchaipichat and Khalili (2009) indicates that the shear stress-strain curves of soil are affected by temperature, it is assumed in this study that the Q-z and T-z curves do not depend on temperature. The curves shown in Figure 4.4 are the same curves used by McCartney and Rosenberg (2011) in their load transfer analysis involving energy foundations in Bonny silt.

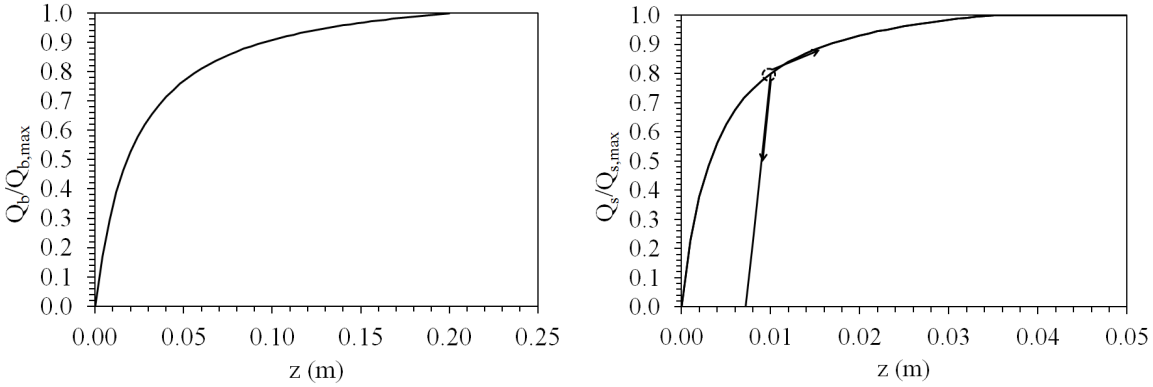

Figure 4.4: Load-transfer curves: (a) Q-z curve; (b) T-z curve

The Q-z and T-z curves in Figure 4.4 are represented in this study using hyperbolic equations for simplicity. The side shear resistance (Q_s) and the base reaction (Q_{base}) at any relative displacement can be obtained using following equations:

Eq. 4.9
$$Q_{base} = Q_{b,max} \times \frac{\rho_{base}}{a_b + b_b \rho_{base}}$$

Eq. 4.10 $$Q_s = Q_{s,max} \times \frac{\rho_s}{a_s + b_s \rho_s}$$

where a_b, b_b, a_s and b_s can be selected based on the best fit to the experimental data. McCartney and Rosenberg (2011) used parameters for the Q-z and T-z curves of a_b = 0.02, a_s = 0.0035 and b_b = b_s = 0.9 in a simplified thermo-mechanical load transfer analysis involving energy foundations in Bonny silt. These parameters were adopted for use in the parametric evaluation. Eq. 4.10 represents the loading path of the T-z curve used to define the side shear resistance within the foundation for either mechanical analysis or thermo-mechanical analysis below the null point. The unloading path of the T-z curve used for thermo-mechanical analysis for the portion of the foundation above the null point can be defined as follows:

Eq. 4.11 $$Q_s = Q_{s,max} \times \left[\frac{\rho_s}{a_s} + \frac{Q_{s,i}}{Q_{s,max}} - \left(\frac{1}{\frac{Q_{s,max}}{Q_{s,i}} - b_s} \right) \right]$$

where $Q_{s,i}$ represents the initial side shear resistance after the mechanical loading is applied.

CHAPTER 5: Evaluation of the Load Transfer Analysis

This chapter includes an evaluation of the load transfer analysis to assess its capabilities. First, the definition of the null point is evaluated for several simple example cases. These cases provide the limits on the expected locations of the null point. Next, the stress and strain distributions in hypothetical energy foundations are presented to highlight the impact of different boundary conditions which may be encountered in practice. These examples highlight the importance of selecting the building-foundation spring stiffness K_h. Finally, a parametric evaluation of the impact of temperature and friction angle of surrounding soil is presented, as these are vital input parameters in the load transfer analysis.

5.1 Definition of the Null Point Location for Simple Cases

In this section, several examples of simple foundations will be discussed in order to understand the impact of different parameters in defining the null point location. Although it is recommended to use multiple elements in an analysis of a real energy foundation when defining the null point location, two elements are used in the following three examples for transparency and simplicity of calculations. Linear elastic behavior was considered for the materials in the following examples. A typical schematic of an energy foundation with two elements is shown in Figure 5.1, along with the relevant geometric and soil-structure interaction variables. In this schematic, x is the location of the null point from the top of the foundation, which is L-x from the base.

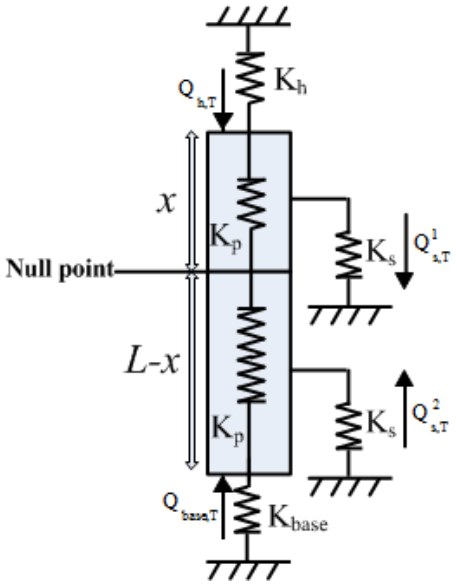

Figure 5.1: Typical foundation schematic along with geometric and resistance load variables (for a foundation under heating)

Example 1) If a foundation which is built in a single layer soil has free boundary condition at the top and the bottom, it represents a condition in which $K_{base} = K_h = 0$ (or $Q_{base,T} = Q_{h,T} = 0$); In this case the null point location will be in the middle of the foundation in such that the side shear resistance for the top section is equal to the side shear resistance of the bottom section as follows.

Eq. 5.1 $$Q_{s1,T} = Q_{s2,T}$$

Considering a uniform linear elastic behavior for the soil surrounding the foundation, the location of the null point will deduced as follows:

Eq. 5.2 $$K_s \frac{\alpha x \Delta T}{2} = K_s \frac{\alpha (L - x) \Delta T}{2}$$

Equation 5.2 will be satisfied when x = L/2. Theoretically, if a foundation located in single layer soil is at the same condition at the top and the bottom in which $K_{base} = K_h \neq 0$, this also satisfies the above equation even if two more terms indicating the extremities reactions should be added o the above equation. The null point will still be located at L/2.

Although these cases may not represent real cases but it is important to see how material rigidity can affect the null point location and the thermal response of the foundation.

Example 2) If a foundation which is built in a single layer soil is free to move from the top but restricted from the bottom, it represents a condition in which $K_h = 0$ (or $Q_h = 0$); In this case two conditions can be assumed specifically: (a) If K_{base} is semi-rigid ($K_{base} > 0$) which represents a case that the foundation sits on a soil with semi-rigid material; (b) If K_{base} is fully rigid ($K_{base} \approx \infty$) which represents a case that the foundation lies on a stiff rock. In case (a), the location of null point can be defined as follows:

Eq. 5.3
$$K_s \frac{\alpha x \Delta T}{2} = K_{base} \alpha (L - x) \Delta T + K_s \frac{\alpha (L - x) \Delta T}{2}$$

By rearranging the terms in Equation 5.3, x can be deduced as follows:

Eq. 5.4
$$x = \frac{K_{base} - \frac{K_s}{2}}{K_{base} + K_s} L$$

According to Eq. 5.1, when K_{base} is assumed to be infinite in case (b), x should be equal to L. This implies that the null point will be located at the base of the foundation.

Example 3) If an energy foundation which is built in a soil restricted from both top and the bottom of the foundation, then the following equation can be used. This condition is representing a real case.

Eq. 5.5
$$K_h \alpha x \Delta T + K_s \frac{\alpha x \Delta T}{2} = K_{base} \alpha (L - x) \Delta T + K_s \frac{\alpha (L - x) \Delta T}{2}$$

by rearranging the terms in Equation 5.5, x can be deduced as follows:

Eq. 5.6
$$x = \frac{K_{base} - \frac{K_s}{2}}{K_{base} + K_s + K_h} L$$

In this equation, both K_{base} and k_h are critical to define the null point location. As mentioned, these simple examples were given to describe that how boundary conditions can change the location of the null point.

5.2 Impact of Axial Boundary Conditions on Thermal Load Transfer Analysis

Three types of boundary conditions for deep foundations are studied in this section: a semi-floating shaft, a floating shaft and an end-bearing shaft. For all three of these boundary conditions, a hypothetical prototype foundation with a length of L = 10 m and a diameter of D = 1 m is used in the analyses. The coefficient of thermal expansion of the shaft is assumed to be $\alpha_T = 10\times10^{-6}$ m/m°C. The unit weight and the Young's modulus of the foundation are assumed to be $\gamma_f = 24$ kN/m^3 and $E_f = 20$ GPa respectively. A soil having a drained friction angle (ϕ_s) of 30° (for the ultimate side shear resistance), unite weight (γ_s) of 18 kN/m^3 and an undrained shear strength of $c_u = 54$ kPa (for the ultimate end bearing) are assumed for the soil surrounding the foundation. The hypothetical Q-z and T-z curves used in the analysis to determine the base reaction (Q_{base}) and the shear resistance (Q_s) are presented separately for each boundary condition case.

4.1.1 Case 1: Semi-Floating Shaft

A semi-floating shaft which supports a building load through both end bearing and side shear resistance is the most common type of deep foundation. In order to define the response of a semi-floating foundation to thermo-mechanical loading, a foundation having the same geometry and soil properties in Section 5.1 along with the following model parameters was evaluated. The building load and the foundation head-structure stiffness were assumed to be P = 500kN and $K_h = 0.5$ GPa/m respectively.

Table 5.1: Model parameters for Case 1: Semi-floating shaft

P (kN)	500
$\phi'(°)$	30
$\Delta T(°C)$	20
K_h(GPa/m)	0.5

The MATLAB code in Appendix A was written to determine the induced stress profiles through a foundation that is loaded mechanically (M), thermally (T), or thermo-mechanically (M+T). The results for this foundation are shown in Figure 5.2 for heating to a temperature difference $\Delta T = 20°C$. As expected, the compressive stress decreases along the foundation when it is loaded mechanically. The amount of imposed tip movement for this example lead to a small mobilization of the end bearing. When the foundation is heated, it expands about its null point, and the highest compressive stresses are noted at this point. As noted in the previous section, the boundary restraints at the top and bottom of the foundation dictate the location of the null point. For the conditions in Table 5.1, the null point was defined at a depth of 4 m from the top of foundation.

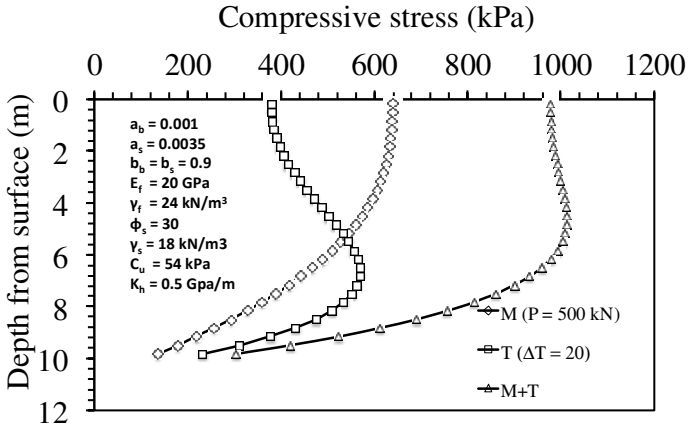

Figure 5.2: Compressive stress vs. depth for a semi-floating shaft under mechanical loading (M), thermal loading (T), thermo-mechanical loading (M+T)

The thermo-mechanical strain of this foundation is shown in Figure 5.3. The results in this figure indicate that the compressive stress and strain are inversely related The lowest value of the thermo-mechanical strain in Figures 5.3 occurs at the null point. Accordingly, the null point has the lowest thermal strain but the highest stress. This is because the soil offers the most resistance to the tendency for the foundation to expand about the null point.

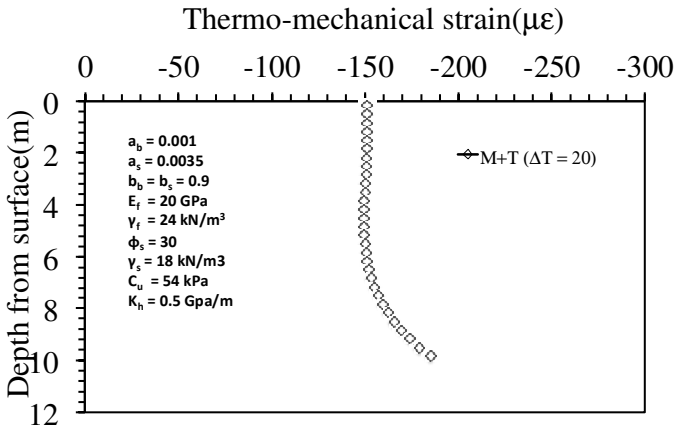

Figure 5.3: Thermo-mechanical strain vs. depth for a semi-floating shaft in Case 1

5.2.2 Case 2: Floating shaft

A floating shaft is one in which the entire building load is supported by the side shear resistance of the shaft and the end bearing is negligible ($K_{base} = 0$). The T-z curve used in this analysis is the same as the previous case. The model parameters are tabulated below. The rest of the parameters are the same as in Case 1.

Table 5.2: Model parameters for Case 2: Floating shaft

P (kN)	500
ϕ'(°)	30
ΔT(°C)	20
K_h(GPa/m)	0.5

According to results, the null point is located at the same position as previous case. This indicates that the mobilized end bearing resistance in previous case is very small and almost negligible. The compressive stress profiles along the foundation are sketched in Figure 5.4 based on the analysis. As seen in this figure, the compressive stress at the top of the foundation for mechanical, thermal and thermo-mechanical analyses is slightly lower than their values in the previous case. The compressive stress at the base of foundation is clearly lower than the previous case as the mobilized end bearing resistance was assumed to be zero in this case.

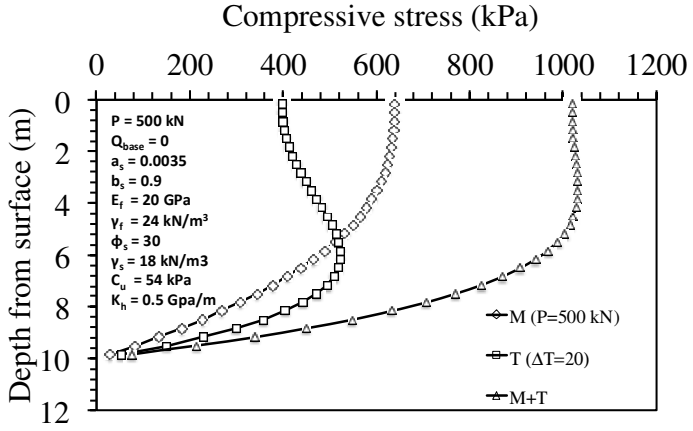

Figure 5.4: Compressive stress vs. depth for a floating shaft under mechanical loading (M), thermal loading (T), thermo-mechanical loading (M+T)

The thermo-mechanical axial strain in the floating shaft is shown in Figure 5.5. As seen in this figure, the strain at the top of the foundation is lower than the bottom due to the confinement of the foundation at the top (ascending trend toward bottom). The confinement at the top of the foundation imposes a higher compressive stress at the foundation butt, which prevents the foundation from free expanding from the top during heating. On the other hand, the bottom of the foundation can expand almost freely as there is negligible confinement at the bottom (i.e., zero end bearing).

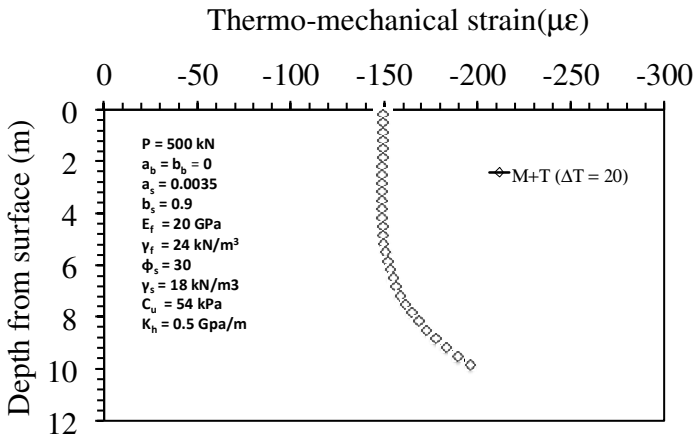

Figure 5.5: Thermo-mechanical strain vs. depth for a floating shaft

5.2.3 Case 3: End-bearing Foundation

An end-bearing foundation is assumed to have negligible side shear resistance (Q_s) along its length, and the applied axial load is supported solely by end bearing. Since no side shear resistance will be mobilized due to mechanical and thermal loading, the compressive stress and the axial strain are constant along the foundation, as shown in Figures 5.6(a) and 5.6(b), respectively. The model parameters are the same as Case 1. In this case, in order to increase the spring stiffness at the bottom $a_b = 0.01$ was used in the Q-z equation. This case is representative of the situation in which the foundation rests on a hard surface (e.g. rock), and the shaft side resistance is negligible.

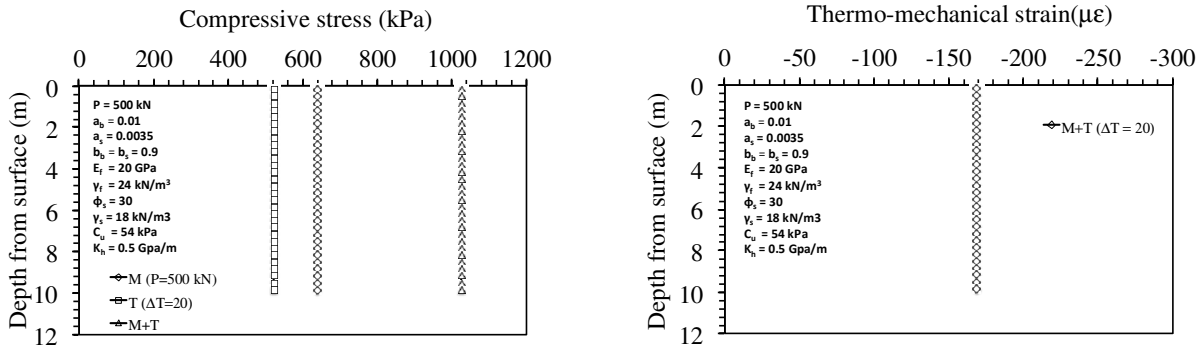

Figure 5.6: Thermo-mechanical results for an end bearing foundation: (a) Compressive stress (b) Thermo-mechanical strain

5.3. Impact of Temperature on the Thermo-Mechanical Response of an Energy Foundation

A semi-floating foundation with the same parameters used in Section 5.2 is considered in this section to evaluate the effect of temperature on thermo-mechanical response of an energy foundation. The results in Figure 5.7 indicate that the axial compressive stress increases proportionally to the temperature. The change in the shape of the curves with temperature is due to the change in ultimate side shear with increasing temperature. For values of ΔT of 5°C and 10°C the maximum stress appears at the top of the foundation and decreases over the depth. It seems that additional axial stresses on the elements due to thermal loading are not very significant and the profile shows almost the same behavior as the foundation is only loaded mechanically but with higher values. As the temperature increases, the temperature impact on the foundation increases apparently such that a sharp peak can be seen in the profile at ΔT = 50°C.

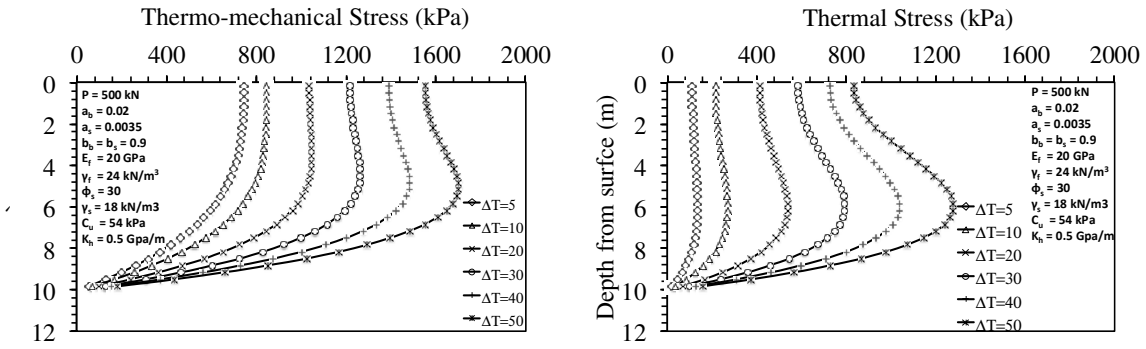

(a) (b)

Figure 5.7: Change in axial stress of a semi-floating shaft in response to different temperatures: (a) Thermo-mechanical; (b) Thermal

The strain response of the foundation for different temperatures is shown in Figure 5.8. The strain is almost constant for small temperature changes and becomes more

nonlinear with increasing temperature changes. This results from the effects of side shear resistance on the foundation performance. The maximum strain at $\Delta T = 50°C$ is 5 times larger than the maximum strain at $\Delta T = 5°C$.

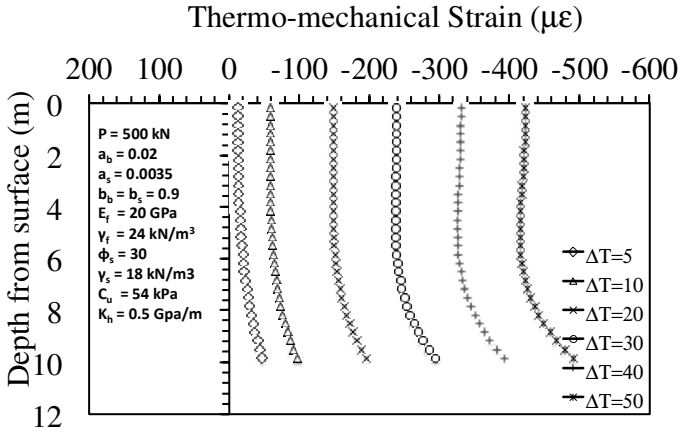

Figure 5.8: Change in axial strain of a semi- floating shaft in response to different temperatures

The maximum axial stress and strain in a semi-floating shaft for different temperature changes is shown in Figure 5.9. The stresses and strains increase linearly with temperature as expected. The maximum axial stress shows almost linear behavior with increasing temperature. The maximum stress in $\Delta T = 50°C$ is about 2 times larger than a foundation that experience a very low temperature change. It is important to assess the change in compressive stress in an energy foundation as it may result in structural distress of the foundation if not properly compared to the confined compressive strength of the foundation.

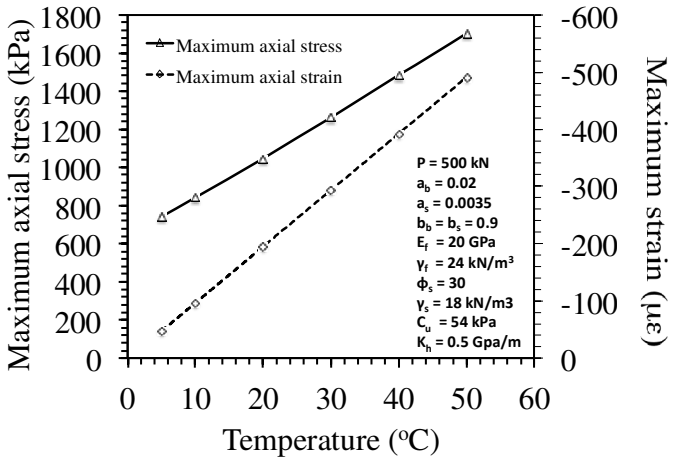

Figure 5.9: Maximum values of stress and strain in a semi-floating foundation at different temperatures

5.4 Impact of Soil Friction Angle on the Thermo-Mechanical Response of an Energy Foundation

Another parameter than can have an effect on the energy foundation's response is the friction angle of the surrounding soil. The reason this parameter was selected to be studied among other parameters of the soil is that the ultimate shear resistance and consequently the mobilized shear resistance of the foundation are directly related to the friction angle of the soil according to the β method (Coduto 2006) and the changes in ultimate side shear during temperature changes (Rosenberg 2010). A semi-floating foundation with the same parameters used in Section 5.2 and friction angles ranging from 20° to 40° are considered in the analysis. The results are shown in Figure 5.10. The results indicate the trend in the maximum axial strain with temperature is non-linear. The maximum stress and the minimum strain occur for soils with the highest friction angle. The results can also help a designer predict the thermo-mechanical response of a similar foundation for different soils having different friction angles.

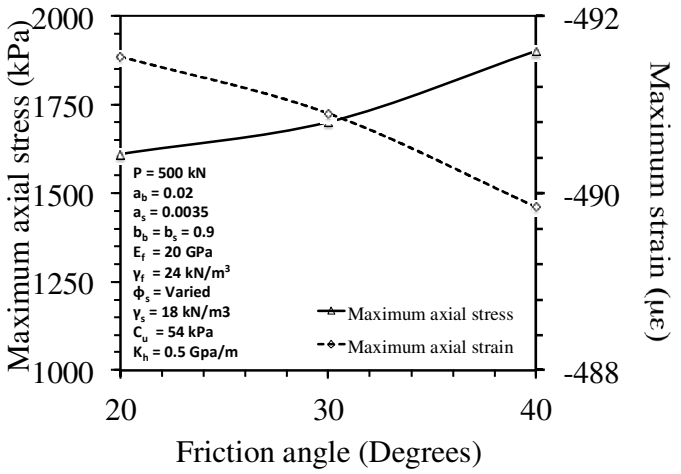

Figure 5.10: Impact of the soil friction angle on the thermo-mechanical behavior of a floating foundation: (a) Axial thermal stress (b) Axial thermal strain

5.5 Impact of Head-Structure Stiffness on the Thermo-Mechanical Response of an Energy Foundation

Another parameter than can have an effect on the energy foundation's response is the head-structure stiffness (K_h). This parameter is used to define the null point location. A semi-floating foundation with the same parameters used in Section 5.2 is considered in this analysis to investigate the effect of head-structure stiffness on thermo-mechanical response of an energy foundation.

The results of analysis for four different values of head-structure stiffness for a temperature change of 20 °C can be seen in Figure 5.11. The null point, which corresponds to the maximum axial stress and minimum axial strain within the foundation moves upward as the magnitude of K_h increases. For the particular soil and foundation properties, the maximum axial stress and minimum axial strain occurs when K_h equals 13 GPa, at in which case the null point is located at the ground surface. The thermo-mechanical stresses and strains in Figures 5.11(a) and 5.11(b) reflect the combined effect

of thermal and mechanical loading, while the thermal stresses and strains in Figures 5.11(c) and 5.11(d) reflect the isolated effect of thermal loading. The null point can be seen more obviously when examining the thermal stresses alone.

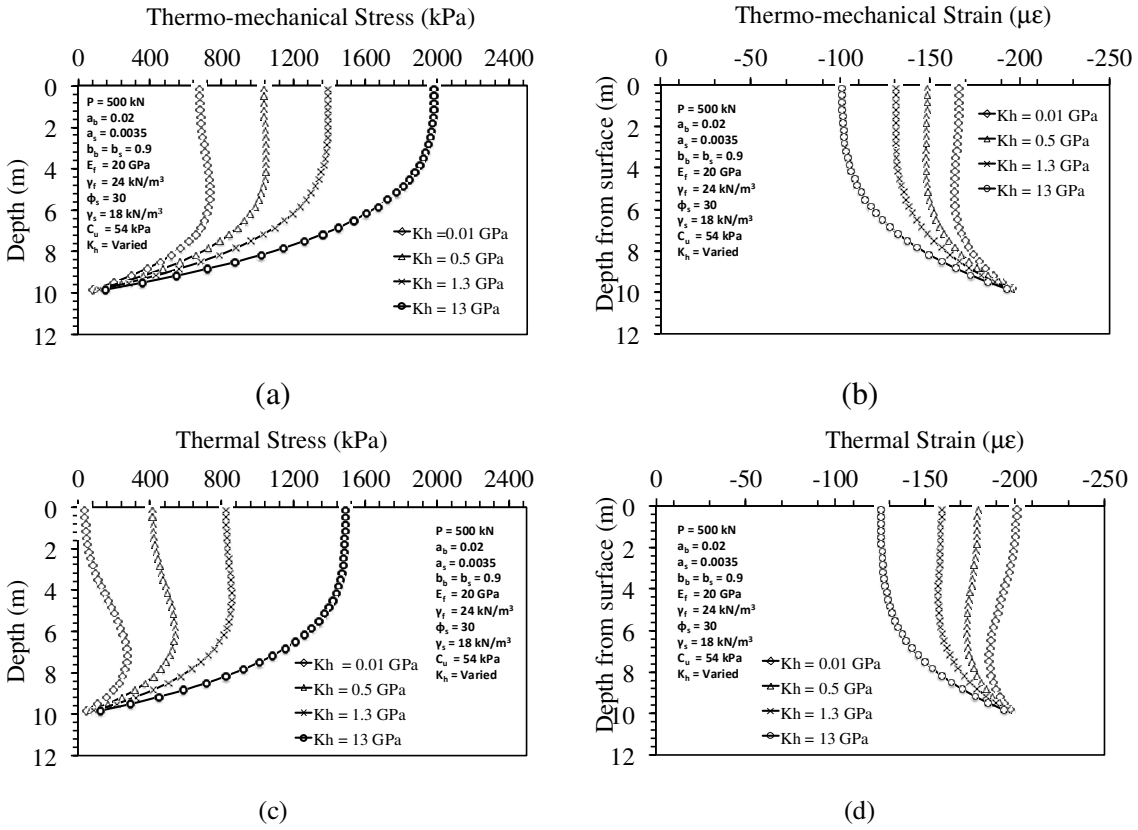

Figure 5.11: Impact of the head-structure stiffness (K_h) on the thermo-mechanical behavior of a floating foundation: (a) Thermo-mechanical stress (b) Thermo-mechanical strain (c) Thermal stress (d) Thermal strain

CHAPTER 6: Validation of the Load Transfer Analysis

The results of a centrifuge-scale model energy foundation test are used in this chapter for the purpose of validating the load-transfer analysis developed in this study. The details of the centrifuge testing setup and procedures are presented in detail by Stewart and McCartney (2012), and the results are presented in Stewart (2012).

6.1 Model Foundation Description

A small-scale model foundation with dimensions of 50.8 mm in diameter and 533.4 mm in length was tested in the centrifuge at a g-level of 24.6. This model foundation indicates that the stresses and strains induced in the foundation are representative of a prototype foundation which has a diameter of 1.25 m and a length of 13.12 m. These dimensions are typical for drilled shafts used in building support applications for 2-3 story buildings. Pictures of the completed scale model foundation and a schematic showing the dimensions of the instrumentation locations are shown in Figures 6.1(a) and 6.1(b).

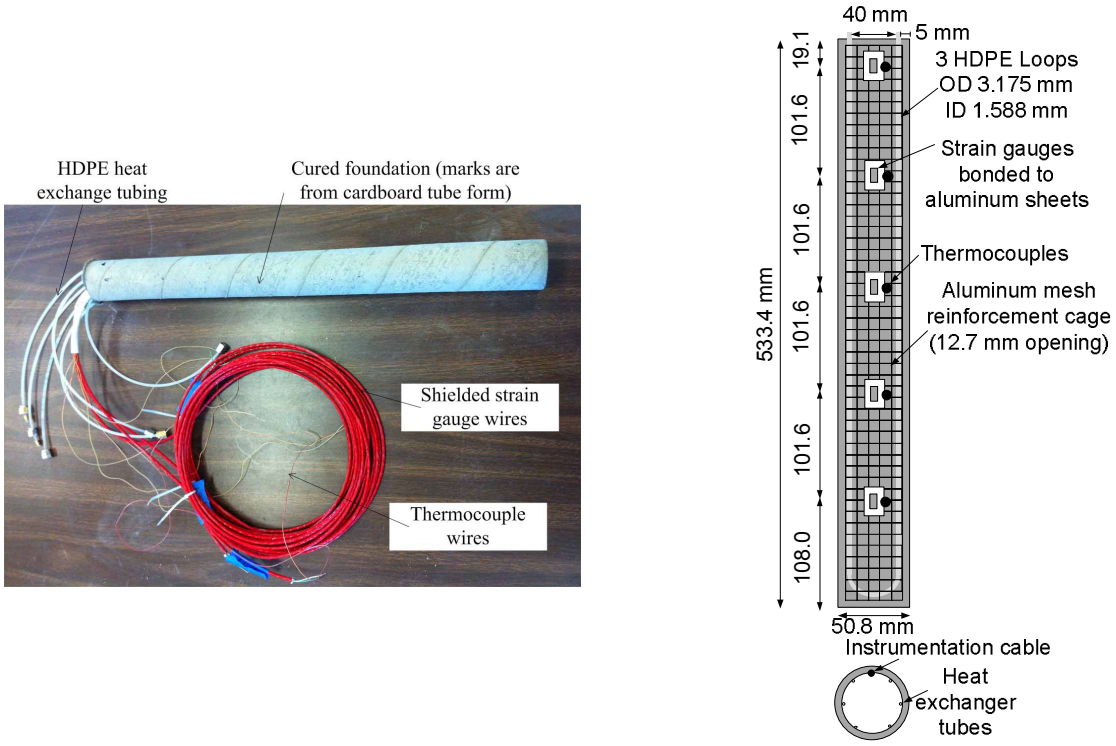

(a) (b)

Figure 6.1: (a) Scale model foundation; (b) Schematic with instrumentation layout (Stewart and McCartney 2012)

Before centrifuge testing, a comprehensive set of characterization tests were performed on the pre-cast foundation outside of the soil in a load frame at 1-gravity to determine its mechanical and thermal properties. The coefficient of thermal expansion (α) was estimated 9.69×10^{-6} m/m°C. Also, the secant elastic modulus of foundation (E) was estimated 7.17 GPa based on the tests. The value of E is smaller than that of the reinforced concrete in energy foundations because the amount of coarse aggregate was lower in the reinforced concrete of the model foundation.

5.2 Centrifuge Test Description

A cylindrical container with 13 mm-thick insulation sheet wrapped around the container used in this test along with its dimensions is shown in Figure 6.2. The

foundation evaluated in this study is an end-bearing foundation, with the tip resting on the rigid steel base plate of the container.

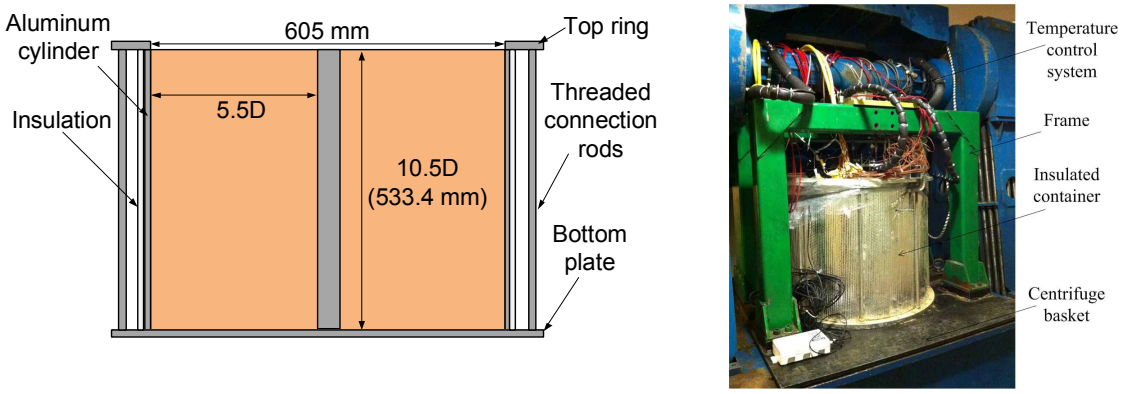

Figure 6.2: Schematic of the model, container and load frame used in centrifuge testing (Stewart and McCartney 2012)

The instrumentation incorporated into the centrifuge container is shown in Figure 6.3. Four linear variable differential transformers (LVDT's) were placed on top of the foundation and on the soil surface at three different radial distances from the foundation. These LVDT's were used to profile the settlement basin created by movement of the foundation in the soil. Four thermocouple profile probes were inserted into the soil at different radial locations from the foundation. Each of the profile probes was equipped with 6 thermocouples at varying depths along the probe. These probes were used to measure the transient temperature in the soil surrounding the foundation to assess heat transfer outward from the foundation. Water content sensors were placed in the soil around the foundation during the compaction phase of sample preparation at different depths. These sensors were used to track changes in moisture content corresponding with heat flow through the soil specimen. Five universal linear-pattern strain gauges were attached to the metal reinforcement cage embedded in concrete at different depths in the

foundation. At each of these strain gauges locations, a thermocouple was placed as well to track the foundation temperature corresponding to the strain gauge measurements.

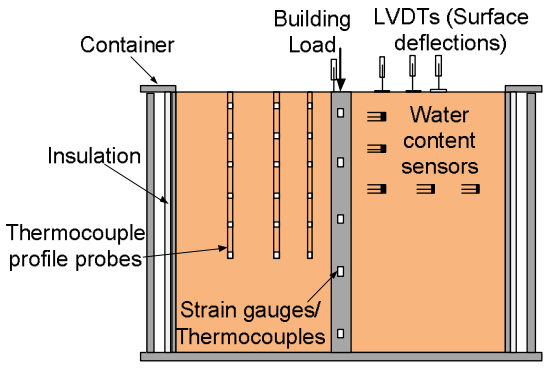

Figure 6.3: Section of instrumentation layout (Stewart and McCartney 2012)

A heat pump was used to control the temperature within the scale-model foundations. The heat pump was connected to the foundation via the hydraulic slip ring stack as shown in Figure 6.4 (Stewart and McCartney 2012).

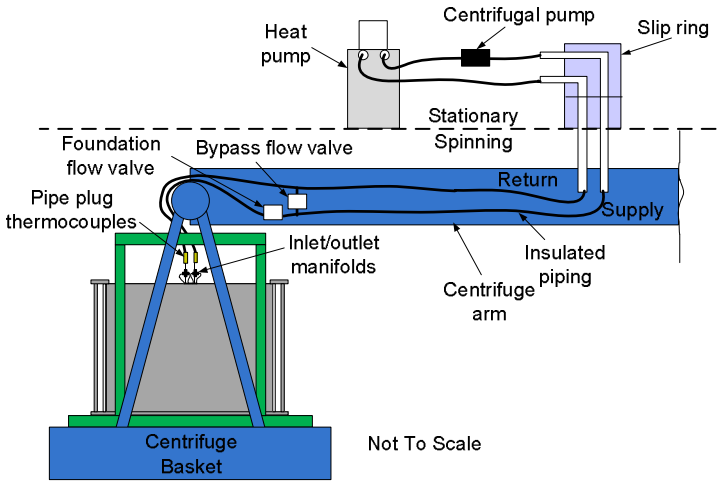

Figure 6.4: Heat pump and control system (Stewart and McCartney 2012)

6.3 Soil Description

Soil obtained from the Bonny dam near the Colorado-Kansas border was used in the energy foundation modeling tests in this study. The liquid and plastic limits of the soil measured according to ASTM D4318 were found to be 26 and 24. As the fines content of

this soil is 84%, this soil classifies as ML (inorganic silt) according to the Unified Soil Classification System (USCS). The silt has a specific gravity G_s of 2.6. The soil is unsaturated and compacted with the dry density of 1451 kg/m^3. The c/p ratio of the soil was estimated equal to 0.45 according to a CU triaxial test on Bonny silt for this dry density. The drained friction angle was also estimated equal to 29° based on the same test.

6.4 Centrifuge Testing Results

The centrifuge tests on the small-scale foundation were performed to investigate the effect of temperature on the strain distribution in the energy foundation during heating. The centrifuge results from heating of the foundation to different temperatures re shown in Figure 6.5. An axial stress of 440 kPa was applied before heating. These results indicate that the maximum thermal axial stress in the foundation was at the center of the foundation. The results indicate that heating led to an increase in axial thermal stress of more than 30 times the mechanical axial stress. The increase in axial stress greater than the applied mechanical stress is possible because of the restraint of the foundation. At ΔT=19 °C the maximum compressive stress is almost 7 times larger than the maximum axial stress at ΔT=5 °C. This indicates that the temperature change during the application of energy foundation may have a significant effect on the thermal response of an energy foundation that needs to be investigated further. The overall trend of the axial compressive stress profiles is consistent with the results observed in semi-floating foundation in Section 5.3.

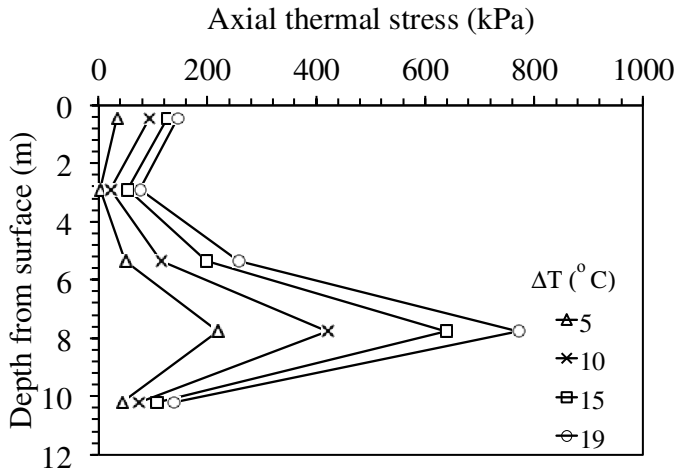

Figure 6.5: Axial compressive stress profiles in different temperature changes for the centrifuge model foundation

6.5 Load-Transfer Model Analysis

The centrifuge small-scale foundation data was used to validate the load-transfer model presented in this research. The model parameters from Stewart and McCartney (2012) are summarized in Table 6.1

Table 6.1: Model parameters

Foundation Geometry	
L (m)	13.1
D (m)	1.2
Soil Properties	
ϕ'(°)	29
c/p ratio	0.435
γ (kN/m^3)	15.7
Foundation Parameters	
α (m/m°C)	9.69×10^{-6}
E (GPa)	7.17
γ (kN/m^3)	24

The shape of the Q-z and T-z curves used in this model are represented by the hyperbolic model used by McCartney and Rosenberg (2011). The fitting parameters for the Q-z curve of $a_b = 0.002$ and $b_b = 0.9$ were used in this analysis to represent the stiff

end restraint at the tip of the foundation, which is the same as that used by McCartney and Rosenberg (2011). The parameters of the T-z curve were a_s = 0.0035 and b_s= 0.9, The axial thermal expansion of the foundation outside of the soil measured under application of different temperatures was used to define the value of the stiffness of head-structure stiffness (K_h). The value of K_h that provided the best fit to the data was 0.1 GPa/m (Stewart 2012).

The predicted axial compressive stress profiles using load-transfer model analysis along with the centrifuge data for each temperature change condition are shown in Figures 6.6(a) through 6.6(d). The results in these figures indicate that the new thermo-mechanical load transfer analysis provided good estimate of axial compressive stress induced by the thermal loading in the energy foundation studied in this research. The overall trend from the model is the same as the centrifuge data. However, the peak value of the axial stress profile for the centrifuge data is higher than the model.

Overall, the results of the load-transfer model shows promise as an approach to provide an estimate for the thermal analysis of an energy foundation. However, in order to completely validate this model, more experiments at model or prototype-scale with different boundary conditions and soil conditions (i.e., different degrees of saturation, densities, etc.) are needed for comparison purposes. This will also help refine the relationships for the end bearing and side shear presented in Chapter 4.

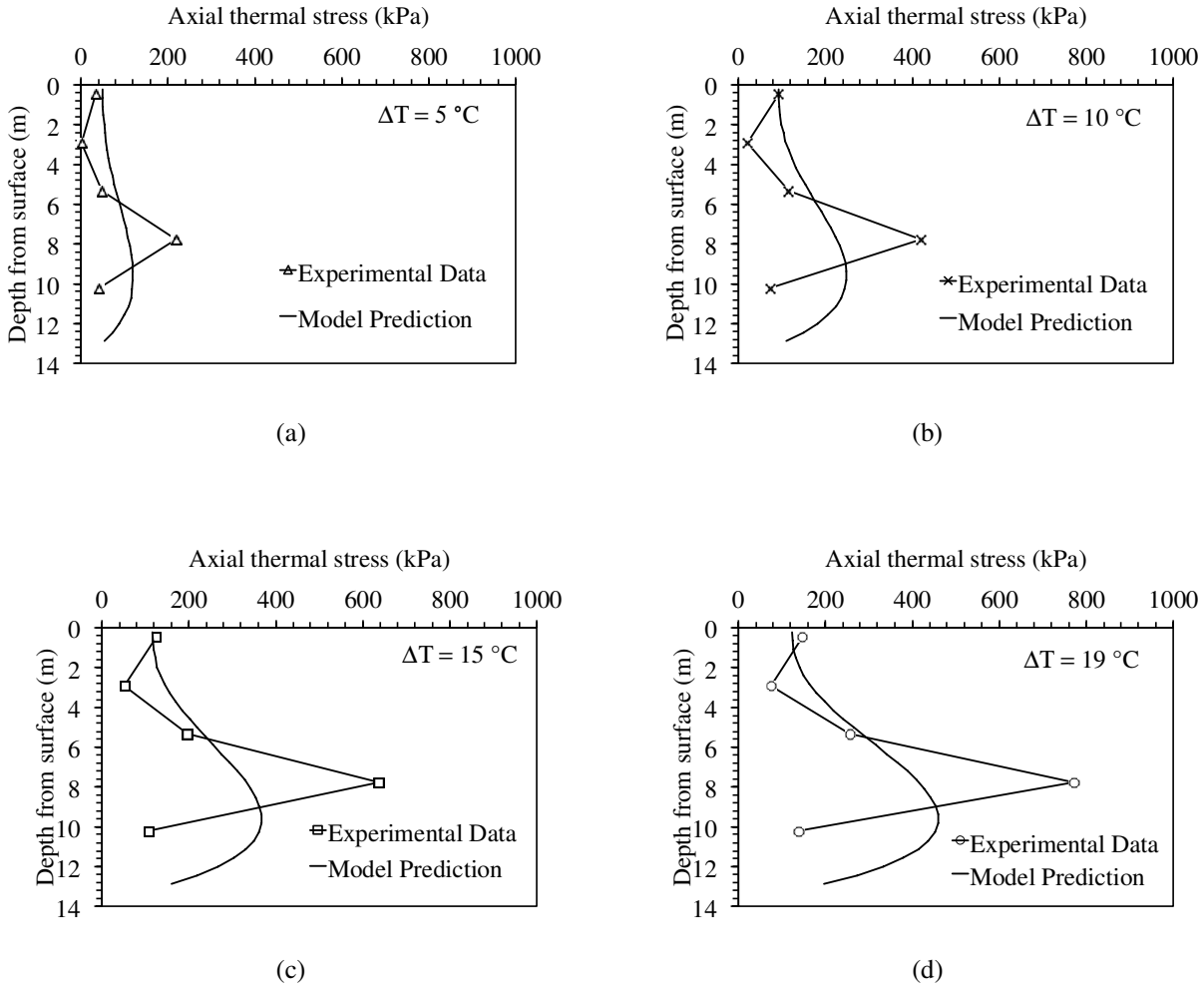

Figure 6.6: The comparison between the model prediction and the experimental data at (a) ΔT = 5°C; (b) ΔT = 10°C; (c) ΔT = 15°C; (d) ΔT = 19°C

CHAPTER 7: Conclusion

This study involved the development of a new load-transfer analysis that accounts for the complex interaction between soils and foundations during mechanical and thermal loading. The analysis of some representative cases (floating, semi-floating and end bearing shaft) indicated that during heating, the foundation tended to expand about the null point. Because the soil side shear resistance opposed the thermal expansion of the foundation, compressive axial stresses were generated in the foundation which had the maximum magnitude in the null point. The null point location was defined for some simple cases to investigate that effect of boundary conditions on the location of the null point. The impact of the temperature changes and also the friction angle of the surrounding soil were studied in this research. The results implied that the higher the temperature changes, the higher the axial stresses and strains are expected to be generated in the energy foundation. The increase of ultimate side shear resistance due to the radial expansion of the foundation during heating was implemented in the analysis. A method was suggested in this research that accounts for the effect of mechanical loading on the increase of end bearing resistance for a foundation which is heated. The model analysis was validated based on a centrifuge test on a scale-model foundation. The T-z model analysis provided good estimate of axial compressive stress induced by the different thermal loadings in the foundation studied in this research. Overall, the application of the load-transfer analysis to evaluate the impacts of heating shows promise, but needs to be investigated further.

REFERENCES

Abuel-Naga, H. M, Bergardo, D. T., Bouazza, A., and Pender, M. (2009). "Thermomechanical model for saturated clays." Géotechnique. 59(3), 273–278.

Adam, D. and Markiewicz, R. (2009). "Energy from earth-coupled structures, foundations, tunnels and sewers." Géotechnique. 59(3), 229–236.

Amis, T., Bourne-Webb, P.J., and Amatya, B. (2009). "Geothermal business buoyant." Geodrilling International. Issue 148.

Boënnec, O. (2009). "Piling on the energy." Geodrilling International.

Bourne-Webb, P.J., Amatya, B., Soga, K., Amis, T., Davidson, C. and Payne, P. (2009). "Energy pile test at Lambeth College, London: Geotechnical and thermodynamic aspects of pile response to heat cycles." Geotechnique. 59(3), 237–248.

Brandl, H. (2006). "Energy foundations and other thermo-active ground structures." Géotechnique. 56(2), 81-122.

Choi, J.H., and Chen, R.H.L. (2005). "Design of continuously reinforced concrete pavements using glass fiber reinforced polymer rebars." Publication No. FHWA-HRT-05-081. Washington, D.C.

Coccia, C.J., Rosenberg, J.E., and McCartney, J.S. (2011). "Soil structure interaction in geothermal foundations." Proceedings of 2011 NSF CMMI Engineering Research and Innovation. January 4-6th 2011. Atlanta, GA.

Coyle, H.M., and Reese, L.C. (1966). "Load transfer for axially loaded piles in clay," Proceedings, American Society of Civil Engineers, New York, NY. 92(SM2), 1-26.

Ennigkeit, A. and Katzenbach, R. (2001). "The double use of piles as foundation and heat exchanging elements." Proceedings 15th International Conference on Soil Mechanics and Geotechnical Engineering. Istanbul, Turkey. p. 893-896.

Knellwolf, C., Peron, H., and Laloui, L. (2011). "Geotechnical analysis of heat exchanger piles." Journal of Geotechnical and Geoenvironmental Engineering. ASCE. 137(12), 890-902.

Laloui, L. (2011). "In-situ testing of heat exchanger pile." Geo-Frontiers: Advances in Geotechncial Engineering. Proceedings of the Geo-Frontiers 2011 Conference. Dallas, TX. 10 pg.

Laloui, L., Nuth, M., and Vulliet, L. (2006). "Experimental and numerical investigations of the behaviour of a heat exchanger pile." IJNAMG. 30, 763–781.

Laloui, N. and Nuth, M. (2006). "Numerical modeling of some features of heat exchanger pile." Foundation Analysis and Design: Innovative Methods (GSP 153). ASCE. Reston, VA. pp. 189-195.

McCartney, J.S., LaHaise, D., LaHaise, T., and Rosenberg, J.E. (2010). "Application of geoexchange experience to geothermal Foundations." ASCE Geotechnical Special Publication 198: The Art of Foundation Engineering Practice. Feb. 20-24, 2010.

McCartney, J.S. and Rosenberg, J.E. (2011). "Impact of heat exchange on side shear in thermo-active foundations." Geo-Frontiers: Advances in Geotechnical Engineering. Dallas, TX. 10 pg.

Ooka, R., Sekine, K., Mutsumi, Y., Yoshiro, S. SuckHo, H. (2007). "Development of a ground source heat pump system with ground heat exchanger utilizing the cast-in place concrete pile foundations of a building." EcoStock 2007. 8 pp.

Peron, H., Knellwolf, C., and Laloui, L. (2011). "A method for the geotechnical design of heat exchanger piles." Geo-Frontiers: Advances in Geotechnical Engineering. Proceedings of the Geo-Frontiers 2011 Conference. Dallas, TX. 10 pg.

Reese, L.C., Isenhower, W.M. and Wang, S.-T. (2006). Analysis and Design of Shallow and Deep Foundations. Wiley Interscience. New York.

Reese, L.C. and O'Neill, M. (1988). Drilled Shafts. Pub. FHWA-HI-88-042. USDOT.

Rosenberg, J.E. (2010). Centrifuge Modeling of Soil Structure Interaction in Thermo-Active Foundation. M.S. Thesis. University of Colorado Boulder

Stewart, M.A. and McCartney, J.S. (2012). "Strain distributions in centrifuge model energy foundation." GeoCongress 2012. Oakland, CA. March 28-30, 2012. 10 pg.

Stewart, M. (2012). Centrifuge Modeling of Strain Distributions in Energy Foundations. MS Thesis. University of Colorado Boulder.

Wood, C.J., Liu, H. and Riffat, S.B. (2009). "Use of energy piles in a residential building, and effects on ground temperature." Geotechnique. 59(3), 287-290.

Zitz, W. and McCartney, J.S. (2011). "Issues in the installation of energy foundations." 2011 SME Annual Meeting. Denver, CO. March 1-3, 2011. 10 pg.

```
%                              APPENDIX A:
%     THERMO-MECHANICAL LOAD-TRANSFER ANALYSIS FOR ENERGY FOUNDATIONS
%
% This program performs T-z analyses for an energy foundation
% under "Thermo-mechanical loading" based on the Beta method.
clear all
format long e
%%-------------------------------------------------------------------------
-%
%%--------------------------------INPUT PARAMETERS
%%-------------------------------------------------------------------------
-%
%% SOIL DESCRIPTION %%
cop = 0.3; %c/p ratio
gamsoil = 18;%KN/M3
Phi = 30; %Drained friction angle
%% FOUNDATION DESCRIPTION %%
L = 10;%m
D = 1; %m
E = 20000;%MPa
gampile =  24;%KN/m3
alphat = 10e-6; %Coeffcient of thermal expansion for R
%% MECHANICAL LOADING%%
P = 500;%KN
%% TEMPERATURE CHANGE %%
deltat = 20;
%-------------------------------------------------------------------------
-%
%% BETA METHOD PARAMETERS %%
beta =0.55; %Emperical reduction factor
k = 65; %emperical coefficient representing the soil resistance to
expansion of the foundation
%% END BEARING FITTING PARAMETERS
ab = 0.02;
bb = 0.9;
%% SHEAR RESISTANCE FITTING PARAMETERS
as = 0.0035;
bs = 0.9;
%% HEAD-STRUCTURE STIFFNESS
Kh=300000;%KN/m (0.5 GPa/m for this case)
%% NUMBER OF ELEMENTS %%
N = 30;
%-------------------------------------------------------------------------
-%
%%
Ab = pi*D^2/4; % m2 - Cross-sectional area
Cs = pi*D; %m - Circumference of pile
Wpile = gampile*Ab*L; %KN - Weight of pile
Wdisp = gamsoil*Ab*L; %kN - Weight of soil displaced
Wp = Wpile - Wdisp; %kN - Buoyant unit weight of pile
%-------------------------------------------------------------------------
-%
%-------------------------------------------------------------------------
-%
%% MECHANICAL TZ ANALYIS BASED ON "P" %%

% ULTIMATE SIDE SHEAR RESISTANCE %
K0=1-sin(Phi*pi/180); %Coefficient of lateral earth pressure at rest
dL =L/N; %m - Length of each soil sublayer
h = 0:dL:L; %m - Depth vector, z=0 at ground surface
zmid = h(1:length(h)-1)+dL/2; %m - Depth of each soil sublayer
sigv = gamsoil*zmid; %m - Effecive vertical stress
fsM = beta*sigv*K0*tan(Phi*pi/180); %KN/m2
As = Cs*dL*ones(length(zmid),1);%m2
```

```
QsM = fsM.*As'; %kN
QstotM = sum(QsM); %kN

% ULTIMATE END BEARING%
sc = 1.2;
dc = 1.5;
Nc = 5;
cub = L*gamsoil*cop; %KN/m2
Qp = cub*Ab*sc*dc*Nc; %kN

% ULTIMATE CAPACITY
QuM = Qp + QstotM - Wp; %kN

n = 1:1:N;
Li = L/N; %m
z = Li*(n-.5); %m
Ki = Ab*E*1000/Li; %KN/m
QbM = zeros(N,1);
QtM = zeros(N,1);
FsM = zeros(N,1);
FsmaxM = zeros(N,1);
pbM = zeros(N,1);
ptM = zeros(N,1);
psM = zeros(N,1);
QaveM = zeros(N,1);
deltaM = zeros(N,1);
sM = zeros(N,1);
sigmaM = zeros(N,1);
pb = 0;
Dtot = 100;
tol = 1e-6;
PDif = 500; % Previous Difference
CDif = 500; % Current Difference
FsmaxM(1)=QsM(1);
for k=2:1:N
    FsmaxM(k)=FsmaxM(k-1)+QsM(k);
end
wxyz = 0;
while abs(CDif)<= abs(PDif)
    wxyz = wxyz + 1;
for i = N:-1:1
    if i == N
        deltaQt = 10; %Initialize while loop
        QtM(i) = 0;
        pbM(i) = pb;
        QbM(i)=Qp*pbM(i)/(ab+pbM(i)*bb);
        %QbM(i)=0;
        while deltaQt > tol
            QaveM(i) = (QtM(i)+QbM(i))/2;
            deltaM(i) = QaveM(i)/Ki;
            ptM(i) = pbM(i) + deltaM(i);
            psM(i) = pbM(i) + deltaM(i)/2; % pt +(pt-pb)/2;
            FsM(i) = FsmaxM(i)*psM(i)/(as+psM(i)*bs);
            QtnewM(i) = FsM(i) + QbM(i);
            deltaQt = QtnewM(i) - QtM(i);
            QtM(i) = QtnewM(i);
            sM(i) = deltaM(i)*1e6/Li;% micro starin
            sigmaM(i) = QaveM(i)/Ab;
        end

    else
        deltaQt = 10; %Initialize while loop
        pbM(i) = ptM(i+1);
        QbM(i) = QtM(i+1);
```

```
        QtM(i) = 0;
        while deltaQt > tol
            QaveM(i) = (QtM(i)+QbM(i))/2;
            deltaM(i) = QaveM(i)/Ki;
            ptM(i) = pbM(i) + deltaM(i);
            psM(i) = pbM(i) + deltaM(i)/2;
            FsM(i)=FsmaxM(i)*psM(i)/(as+psM(i)*bs);
            QtnewM(i) = FsM(i) + QbM(i);
            deltaQt = QtnewM(i) - QtM(i);
            QtM(i) = QtnewM(i);
            sM(i) = deltaM(i)*1e6/Li;
            sigmaM(i) = QaveM(i)/Ab;
        end

    end

end
i=1:1:N;
FsMtot = sum(FsM(i));
PDif = CDif;
CDif = P-FsMtot-QbM(N);
disp('CDif');
disp(CDif);
disp('PDif');
disp(PDif);
pb=pb+1e-6;
end

pb=pb-1e-6;
disp('pb');
disp(pb);
% % %%%%%%%%%%%%%%%%%%%%%%%%%%%%%%%%%%%%%%%%%%%%%%%%%%
% % --------------------------------------------------------------------
----%
%% NULL POINT LOCATION %%
Kp = (1+sin(Phi*pi/180))/(1-sin(Phi*pi/180)); %Coefficient of passive
earth pressure
KT = k*alphat*deltat*(D/2)/(0.02*L); %
fsT = beta*sigv*(K0+(Kp-K0)*KT)*tan(Phi*pi/180); %KN/m2
As = Cs*dL*ones(length(zmid),1); %m2
QsT = fsT.*As'; %kN
QstotT = sum(QsT); %kN
% ULTIMATE CAPACITY %
QuT = Qp + QstotT - Wp; %kN
fmaxT = fsT; %kN
DdeltaTb = 1;
DdeltaTt = 1;
tol = 1e-5;
QtT = zeros(N,1);
QbT = zeros(N,1);
FsT = zeros(N,1);
FsmaxT = zeros(N,1);
psT = zeros(N,1);
pbT = zeros(N,1);
ptT = zeros(N,1);
QaveT = zeros(N,1);
deltaT = zeros(N,1);
sigmaT = zeros(N,1);
sT = zeros(N,1);

FsmaxT(1)=QsT(1);
for k=2:1:N
    FsmaxT(k)=FsmaxT(k-1)+QsT(k);
end
```

```
% BOTTOM SECTION
for m = 1:1:N-1
disp(m)
    DdeltaTb = 100;
    DdeltaTt = 100;
    for k = 1:1:N
        deltaT(k) = Li*alphat*deltat;
    end
    while abs(DdeltaTb)>tol
        for i = N:-1:m
            for j = m:1:N
                if j == m
                    ptT(j) = 0;
                    psT(j) = deltaT(j)/2;
                    pbT(j) = deltaT(j);
                    FsT(j) = FsmaxT(j)*psT(j)/(as+psT(j)*bs);
                    if i==j
                        QbT(j) = QtT(j+1);
                        QtT(j) = QbT(j)+FsT(j);
                        QaveT(j) = (QbT(j)+QtT(j))/2;
                        SigmaT(j,m) = QaveT(j)/Ab;
                        sigmaT(j) = QaveT(j)/Ab;
                        deltanewT(j) = Li*alphat*deltat-
sigmaT(j)*Li/(E*1000);
                        DdeltaTb = deltaT(j)-deltanewT(j);
                        deltaT(j) = deltanewT(j);
                        sT(j) = deltaT(j)*1e6/Li;%micro strain
                        ST(j,m) = deltaT(j)*1e6/Li;
                    end

                elseif j<N
                    ptT(j) = pbT(j-1);
                    psT(j) = ptT(j)+deltaT(j)/2;
                    pbT(j) =  ptT(j)+deltaT(j);
                    FsT(j) = FsmaxT(j)*psT(j)/(as+psT(j)*bs);

                    if i==j
                        QbT(j) = QtT(j+1);
                        QtT(j) = QbT(j)+FsT(j);
                        QaveT(j) = (QbT(j)+QtT(j))/2;
                        SigmaT(j,m) = QaveT(j)/Ab;
                        sigmaT(j) = QaveT(j)/Ab;
                        deltanewT(j) = Li*alphat*deltat-
sigmaT(j)*Li/(E*1000);
                        deltaT(j) = deltanewT(j);
                        sT(j) = deltaT(j)*1e6/Li;
                        ST(j,m) = deltaT(j)*1e6/Li;
                    end

                else
                    if i==j
                        ptT(j) = pbT(j-1);
                        psT(j) = ptT(j)+deltaT(j)/2;
                        pbT(j) = ptT(j)+deltaT(j);
                        FsT(j) = FsmaxT(j)*psT(j)/(as+psT(j)*bs);
                        QbT(j) = Qp*pbT(j)/(ab+pbT(j)*bb);
                        %QbT(j) = 0;
                        QtT(j) = QbT(j)+FsT(j);
                        QaveT(j) = (QbT(j)+QtT(j))/2;
                        SigmaT(j,m) = QaveT(j)/Ab;
                        sigmaT(j) = QaveT(j)/Ab;
                        deltanewT(j) = Li*alphat*deltat-
sigmaT(j)*Li/(E*1000);
```

```
                        deltaT(j) = deltanewT(j);
                        sT(j) = deltaT(j)*1e6/Li;
                        ST(j,m) = deltaT(j)*1e6/Li;
                    end
                end
            end
        end
    end


    n = m:1:N;
    FsTb = sum(FsT(n));
    % TOP SECTION
    if m == 2
       while abs(DdeltaTt)>tol
        j = m-1;
        pbT(j) = 0;
        psT(j) = deltaT(j)/2;
        ptT(j) = deltaT(j);
        FsT(j) = FsmaxT(j)*psT(j)/(as+psT(j)*bs);
        QtT(j) = Qp*ptT(j)/(ab+ptT(j)*bb);
        QbT(j) = QtT(j)+FsT(j);
        QaveT(j) =( QbT(j)+QtT(j))/2;
        SigmaT(j,m) = QaveT(j)/Ab;
        sigmaT(j) = QaveT(j)/Ab;
        deltanewT(j) = Li*alphat*deltat-sigmaT(j)*Li/(E*1000);
        DdeltaTt = deltaT(j)-deltanewT(j);
        deltaT(j) = deltanewT(j);
        sT(j) = deltaT(j)*1e6/Li;
        ST(j,m) = deltaT(j)*1e6/Li;
       end

    end
    if m>2

        while abs(DdeltaTt)>tol

            for i = 1:1:m-1
                for j = m-1:-1:1
                    if j == m-1
                        pbT(j) = 0;
                        psT(j) = deltaT(j)/2;
                        ptT(j) = deltaT(j);
                        FsT(j) = FsmaxT(j)*psT(j)/(as+psT(j)*bs);
                        if i==j
                            QtT(j) = QbT(j-1);
                            QbT(j) = QtT(j)+FsT(j);
                            QaveT(j) = (QbT(j)+QtT(j))/2;
                            SigmaT(j,m) = QaveT(j)/Ab;
                            sigmaT(j) = QaveT(j)/Ab;
                            deltanewT(j) = Li*alphat*deltat-
sigmaT(j)*Li/(E*1000);
                            DdeltaTt = deltaT(j)-deltanewT(j);
                            deltaT(j) = deltanewT(j);
                            sT(j) = deltaT(j)*1e6/Li;%micro strain
                            ST(j,m) = deltaT(j)*1e6/Li;
                        end

                    elseif j>1
                        pbT(j) = ptT(j+1);
                        psT(j) = pbT(j)+deltaT(j)/2;
                        ptT(j) = pbT(j)+deltaT(j);
                        FsT(j) = FsmaxT(j)*psT(j)/(as+psT(j)*bs);
```

```
                        if i==j
                            QtT(j) = QbT(j-1);
                            QbT(j) = QtT(j)+FsT(j);
                            QaveT(j) =( QbT(j)+QtT(j))/2;
                            SigmaT(j,m) = QaveT(j)/Ab;
                            sigmaT(j) = QaveT(j)/Ab;
                            deltanewT(j) = Li*alphat*deltat-
sigmaT(j)*Li/(E*1000);
                            deltaT(j) = deltanewT(j);
                            sT(j) = deltaT(j)*1e6/Li;
                            ST(j,m) = deltaT(j)*1e6/Li;
                        end

                    else
                        if i==j

                             pbT(j) = ptT(j+1);
                             psT(j) = pbT(j)+deltaT(j)/2;
                             ptT(j) = pbT(j)+deltaT(j);
                             FsT(j) = FsmaxT(j)*psT(j)/(as+psT(j)*bs);
                            QtT(j) = Kh*ptT(j);
                            QbT(j) = QtT(j)+FsT(j);
                            QaveT(j) = (QbT(j)+QtT(j))/2;
                            SigmaT(j,m) = QaveT(j)/Ab;
                            sigmaT(j) = QaveT(j)/Ab;
                            deltanewT(j) = Li*alphat*deltat-
sigmaT(j)*Li/(E*1000);
                            deltaT(j) = deltanewT(j);
                            sT(j) = deltaT(j)*1e6/Li;
                            ST(j,m) = deltaT(j)*1e6/Li;
                        end
                    end
                end
            end
        end
    end
    p = m-1:-1:1;
        FsTt=sum(FsT(p));
        Difnull(m) = FsTt+QtT(1)-FsTb-QbT(N);
        disp(Difnull(m))

end

x = min (abs(Difnull));

m = 1;
 for i = 1:1:N-1 ;
 if x == abs (Difnull(i));
     m = i;
 end
 end
 disp NULL
 disp(m)

%% THERMAL TZ ANALYSIS
Kp = (1+sin(Phi*pi/180))/(1-sin(Phi*pi/180)); %Coefficient of passive
earth pressure
KT = k*alphat*deltat*(D/2)/(0.02*L); %
fsT = beta*sigv*(K0+(Kp-K0)*KT)*tan(Phi*pi/180); %KN/m2
As = Cs*dL*ones(length(zmid),1); %m2
QsT = fsT.*As'; %kN
QstotT = sum(QsT); %kN
```

```
% ULTIMATE CAPACITY %
QuT = Qp + QstotT - Wp; %kN
fmaxT = fsT; %kN
DdeltaT = 100;
tol = 1e-6;
QtT = zeros(N,1);
QbT = zeros(N,1);
FsT = zeros(N,1);
FsmaxT = zeros(N,1);
psT = zeros(N,1);
pbT = zeros(N,1);
ptT = zeros(N,1);
QaveT = zeros(N,1);
deltaT = zeros(N,1);
sigmaT = zeros(N,1);
sT = zeros(N,1);

FsmaxT(1)=QsT(1);
for k=2:1:N
    FsmaxT(k)=FsmaxT(k-1)+QsT(k);
end

% BOTTOM SECTION
    for k = 1:1:N
        deltaT(k) = Li*alphat*deltat;
    end
    while abs(DdeltaT)>tol
            for i = N:-1:m
                for j = m:1:N
                    if j == m
                        ptT(j) = 0;
                        psT(j) = ptT(j)+deltaT(j)/2;
                        pbT(j) = ptT(j)+deltaT(j);
                        FsT(j) = FsmaxT(j)*psT(j)/(as+psT(j)*bs);
                        if i==j
                            QbT(j) = QtT(j+1);
                            QtT(j) = QbT(j)+FsT(j);
                            QaveT(j) = (QbT(j)+QtT(j))/2;
                            sigmaT(j) = QaveT(j)/Ab;
                            deltanewT(j) = Li*alphat*deltat-
sigmaT(j)*Li/(E*1000);
                            DdeltaT = deltaT(j)-deltanewT(j);
                            deltaT(j) = deltanewT(j);
                            sT(j) = deltaT(j)*1e6/Li;%micro strain
                        end

                    elseif j<N
                        ptT(j) = pbT(j-1);
                        psT(j) = ptT(j)+deltaT(j)/2;
                        pbT(j) = ptT(j)+deltaT(j);
                        FsT(j) = FsmaxT(j)*psT(j)/(as+psT(j)*bs);

                        if i==j
                            QbT(j) = QtT(j+1);
                            QtT(j) = QbT(j)+FsT(j);
                            QaveT(j) = (QbT(j)+QtT(j))/2;
                            sigmaT(j) = QaveT(j)/Ab;
                            deltanewT(j)=Li*alphat*deltat-
sigmaT(j)*Li/(E*1000);
                            deltaT(j) = deltanewT(j);
                            sT(j) = deltaT(j)*1e6/Li;
                        end
```

```
                    else
                        if i==j
                            ptT(j) = pbT(j-1);
                            psT(j) = ptT(j)+deltaT(j)/2;
                            pbT(j) = ptT(j)+deltaT(j);
                            FsT(j) = FsmaxT(j)*psT(j)/(as+psT(j)*bs);
                            QbT(j) = Qp*pbT(j)/(ab+pbT(j)*bb);
                            %QbT(j) = 0;
                            QtT(j) = QbT(j)+FsT(j);
                            QaveT(j) = (QbT(j)+QtT(j))/2;
                            sigmaT(j) = QaveT(j)/Ab;
                            deltanewT(j) = Li*alphat*deltat-
sigmaT(j)*Li/(E*1000);
                            deltaT(j) = deltanewT(j);
                            sT(j) = deltaT(j)*1e6/Li;
                        end
                    end
                end

            end

%% top section
            for j = m-1:-1:1
                if j == m-1
                    pbT(j) = 0;
                    psT(j) = pbT(j)-deltaT(j)/2;
                    ptT(j) = pbT(j)-deltaT(j);
                    FsT(j) = FsmaxT(j)*psT(j)/(as+psT(j)*bs);
                    QbT(j) = QtT(j+1);
                    QtT(j) = QbT(j)+FsT(j);
                    QaveT(j) = (QbT(j)+QtT(j))/2;
                    sigmaT(j) = QaveT(j)/Ab;
                    deltanewT(j) = Li*alphat*deltat-
sigmaT(j)*Li/(E*1000);
                    deltaT(j) = deltanewT(j);
                    sT(j) = deltaT(j)*1e6/Li;

                else
                    pbT(j) = ptT(j+1);
                    psT(j) = pbT(j)-deltaT(j)/2;
                    ptT(j) = pbT(j)-deltaT(j);
                    FsT(j) = FsmaxT(j)*psT(j)/(as+psT(j)*bs);
                    QbT(j) = QtT(j+1);
                    QtT(j) = QbT(j)+FsT(j);
                    QaveT(j) = (QbT(j)+QtT(j))/2;
                    sigmaT(j) = QaveT(j)/Ab;
                    deltanewT(j) = Li*alphat*deltat-
sigmaT(j)*Li/(E*1000);
                    deltaT(j) = deltanewT(j);
                    sT(j) = deltaT(j)*1e6/Li;
                end

            end

        end


% %%%%%%%%%%%%%%%%%%%%%%%%%%%%%%%%%%%%%%%%%%%%%%%%%%%%%%%%%%%%%%%%%%%%%%%
% % ------------------------------------------------------------------------
----%
%% THERMO-MECHANICAL TZ ANALYSIS %%
% bottom section
```

```
tol = 1e-6;
QtMT = zeros(N,1);
QbMT = zeros(N,1);
FsMT = zeros(N,1);
FsmaxMT = zeros(N,1);
psMT = zeros(N,1);
pbMT = zeros(N,1);
ptMT = zeros(N,1);
QaveMT = zeros(N,1);
deltaMT = zeros(N,1);
sigmaMT = zeros(N,1);
sMT = zeros(N,1);
    DdeltaMT = 100;
    for k=1:1:N
        deltaMT(k) = Li*alphat*deltat;
    end

        while abs(DdeltaMT)>tol
            for i = N:-1:m
                for j = m:1:N
                    if j == m
                        ptMT(j) = ptM(j);
                        psMT(j) = ptMT(j)+deltaMT(j)/2;
                        pbMT(j) = ptMT(j)+deltaMT(j);
                        FsMT(j) = FsmaxT(j)*psMT(j)/(as+psMT(j)*bs);
                        if i==j
                            QbMT(j) = QtMT(j+1);
                            QtMT(j) = QbMT(j)+FsMT(j);
                            QaveMT(j) = (QbMT(j)+QtMT(j))/2;
                            sigmaMT(j) = QaveMT(j)/Ab;
                            deltanewMT(j) = Li*alphat*deltat-
sigmaMT(j)*Li/(E*1000);
                            DdeltaMT = deltaMT(j)-deltanewMT(j);
                            deltaMT(j) = deltanewMT(j);
                            sMT(j) = deltaMT(j)*1e6/Li;%micro strain
                        end

                    elseif j<N
                        ptMT(j) = pbMT(j-1);
                        psMT(j) = ptMT(j)+deltaMT(j)/2;
                        pbMT(j) = ptMT(j)+deltaMT(j);
                        FsMT(j) = FsmaxT(j)*psMT(j)/(as+psMT(j)*bs);

                        if i==j
                            QbMT(j) = QtMT(j+1);
                            QtMT(j) = QbMT(j)+FsMT(j);
                            QaveMT(j) = (QbMT(j)+QtMT(j))/2;
                            sigmaMT(j) = QaveMT(j)/Ab;
                            deltanewMT(j)=Li*alphat*deltat-
sigmaMT(j)*Li/(E*1000);
                            deltaMT(j) = deltanewMT(j);
                            sMT(j) = deltaMT(j)*1e6/Li;
                        end


                    else
                        if i==j
                            ptMT(j) = pbMT(j-1);
                            psMT(j) = ptMT(j)+deltaMT(j)/2;
                            pbMT(j) = ptMT(j)+deltaMT(j);
                            FsMT(j) = FsmaxT(j)*psMT(j)/(as+psMT(j)*bs);
                            QbMT(j) = Qp*pbMT(j)/(ab+pbMT(j)*bb);
                            %QbMT(j) = 0;
```

```
                            QtMT(j) = QbMT(j)+FsMT(j);
                            QaveMT(j) = (QbMT(j)+QtMT(j))/2;
                            sigmaMT(j) = QaveMT(j)/Ab;
                            deltanewMT(j) = Li*alphat*deltat-
sigmaMT(j)*Li/(E*1000);
                            deltaMT(j) = deltanewMT(j);
                            sMT(j) = deltaMT(j)*1e6/Li;
                        end
                    end
                end

            end

%% top section
            for j = m-1:-1:1
                if j == m-1
                    pbMT(j) = pbM(j);
                    psMT(j) = pbMT(j)-deltaMT(j)/2;
                    ptMT(j) = pbMT(j)-deltaMT(j);
                    %FsMT(j) = FsmaxT(j)*psMT(j)/(as+psMT(j)*bs);
                    FsMT(j)=FsmaxT(j)*((psMT(j)/as)+(FsM(j)/FsmaxT(j))-
(1/((FsmaxT(j)/FsM(j))-bs))); % Unloading path
                    QbMT(j) = QtMT(j+1);
                    QtMT(j) = QbMT(j)+FsMT(j);
                    QaveMT(j) = (QbMT(j)+QtMT(j))/2;
                    sigmaMT(j) = QaveMT(j)/Ab;
                    deltanewMT(j) = Li*alphat*deltat-
sigmaMT(j)*Li/(E*1000);
                    deltaMT(j) = deltanewMT(j);
                    sMT(j) = deltaMT(j)*1e6/Li;

                else
                    pbMT(j) = ptMT(j+1);
                    psMT(j) = pbMT(j)-deltaMT(j)/2;
                    ptMT(j) = pbMT(j)-deltaMT(j);
                    %FsMT(j) = FsmaxT(j)*psMT(j)/(as+psMT(j)*bs);
                    FsMT(j)=FsmaxT(j)*((psMT(j)/as)+(FsM(j)/FsmaxT(j))-
(1/((FsmaxT(j)/FsM(j))-bs))); % Unloading path
                    QbMT(j) = QtMT(j+1);
                    QtMT(j) = QbMT(j)+FsMT(j);
                    QaveMT(j) = (QbMT(j)+QtMT(j))/2;
                    sigmaMT(j) = QaveMT(j)/Ab;
                    deltanewMT(j) = Li*alphat*deltat-
sigmaMT(j)*Li/(E*1000);
                    deltaMT(j) = deltanewMT(j);
                    sMT(j) = deltaMT(j)*1e6/Li;
                end

            end

        end



%PLOT AXIAL STRESS CURVE%%

figure (1)
 plot(sigmaM,z,sigmaT,z,sigmaMT,z,'-k','linewidth',1.5,'markersize',10)
 set(gca,'YDir','reverse')
 set(gca,'FontName','Times','FontSize',20)
 xlabel('Axial stress (kN)')
 ylabel('Depth (m)')
 hleg = legend ('M','T','M+T');
```

```
set(hleg,'Location','NorthWest')

%%%%%%

figure (2)
plot(sigmaM,z,'--kx','linewidth',1.5,'markersize',10)
set(gca,'YDir','reverse')
set(gca,'FontName','Times','FontSize',20)
xlabel('Axial stress (kN)')
ylabel('Depth (m)')
hleg = legend ('M');
set(hleg,'Location','SouthEast')

%%%%%%

figure (3)
plot(sigmaT,z,'--kx','linewidth',1.5,'markersize',10)
set(gca,'YDir','reverse')
set(gca,'FontName','Times','FontSize',20)
xlabel('Axial stress (kN)')
ylabel('Depth (m)')
hleg = legend ('T');
set(hleg,'Location','SouthEast')

%%%%%%

figure (4)
plot(sigmaMT,z,'--kx','linewidth',1.5,'markersize',10)
set(gca,'YDir','reverse')
set(gca,'FontName','Times','FontSize',20)
xlabel('Axial stress(kN)')
ylabel('Depth (m)')
hleg = legend ('M+T');
set(hleg,'Location','SouthEast')
```